CONSTRUCTION AND TESTING OF A SINGLE MOLECULE AFM AND APPLYING IT TO STUDY MECHANICAL PROPERTIES OF NOTCH PROTEINS

by

ASHIM DEY

B.Sc., University of Calcutta, 2005

A THESIS

submitted in partial fulfillment of the requirements for the degree

MASTER OF SCIENCE

Department of Physics
College of Arts and Sciences

KANSAS STATE UNIVERSITY
Manhattan, Kansas

2010

Approved by:

Major Professor
Dr. Robert Szoszkiewicz

Copyright

ASHIM DEY

2010

Abstract

For proteins in living cells, forces are present at all levels. These range from macroscopic to single molecule levels. Single molecule atomic force microscopy (AFM) in force extension (FX) and force clamp (FC) modes can investigate the mechanical properties of proteins, for example, forces at which proteins unfold, or the kinetics of these processes. In the FX-AFM experiments, proteins are pulled at constant velocity, while in FC-AFM experiments, proteins are pulled at constant force.

This thesis describes i) how a single molecule FX/FC-AFM was constructed using various components, ii) how it was calibrated and tested using $(I27)_4$ polyprotein, and iii) how it was applied to the studies of a Notch construct. Building up the single molecule FX/FC-AFM system opened a path to investigate the mechanical properties of proteins. Such a system was tested on a known protein construct, hence the usage of the $(I27)_4$ polyprotein. The Notch protein is a signaling protein that plays a role in triggering breast cancer. It is believed that understanding the mechanical properties of Notch can help to understand its oncogenic functions.

We have successfully constructed and calibrated the FX/FC-AFM setup. It was found that the AFM worked for the standard calibration protein of $(I27)_4$. The results on a Notch construct revealed our ability to see some conformational transition state in this molecule under force. These results opened a path for further investigations of a Notch construct at various physiologically relevant conditions.

Table of Contents

List of Figures

List of Abbreviations

ADAM　　　　A Distintegrin And Metalloprotease

AFM　　　　Atomic Force Microscope

BW　　　　Bandwidth

DAQ　　　　Data Acquisition Card

EGF　　　　Epidermal Growth Factor like repeats

FRET　　　　Fluorescence Resonance Energy Transfer

FX/FC-AFM　Force Extension/Force Clamp- Atomic Force Microscope

HD　　　　Heterodimerization domain

HEPES　　　Biological buffer containing 4-(2-hydroxyethyl)-1-piperazineethanesulfonic acid

HOPG　　　Highly Ordered Pyrolytic Graphite

I27　　　　27th domain of human cardiac titin

IC　　　　Intermittent-Contact Mode

ICN　　　　Intracellular domain of Notch protein

$\mathcal{L}_c$　　　　a measure of the contour length increment (see section 4.3)

Lc　　　　an increase in the N-C distance of the unfolding Notch protein

LFM　　　　Lateral Force Microscope

LNR　　　　Lin12/Notch Repeats

MT　　　　Magnetic Tweezers

NC　　　　Non-Contact Mode

NRR　　　　Negative Regulatory Region

OT　　　　Optical Trap

PBS　　　　Phosphate buffered saline

PDB　　　　Protein Data Bank

PSPD　　　Position Sensitive Photo Detector

PZT　　　　Piezoelectric Transducer

Residue　　another term for an "amino acid"

SMFS　　　Single Molecule Force Spectroscopy

STM　　　　Scanning Tunneling Microscope

WLC　　　　Worm Like Chain model of polymer elasticity

Acknowledgement

I would like to give my sincere thanks to my major advisor, Dr. Robert Szoszkiewicz. I had the opportunity of being his first graduate student and got his full attention. I appreciate the time he spent with me teaching me the details about Atomic Force Microscope. I also thank Dr. Neelam Khan, a post-doc in my lab for useful discussion on my work and Scott Chainey for advising me on electronic circuit. I am thankful to our collaborators, Dr. Anna Zolkiewska and Dr. Michal Zolkiewski for providing us with proteins and Dr. Jianhan Chen for simulation study of Notch protein. My sincere thanks go to Dr. Bret Flanders and Dr. Brian Washburn for being my committee members and guiding me through. Also, I would like to thank Josh Lewis for helping me with proofreading and editing and Jacek Szczerbinski for critical comments on my power point presentation.

Last, but not the least, I thank my parents, relatives, friends and colleagues for support and encouragement to me of pursuing my interests.

Dedication

This thesis is dedicated to my dad, Sri Manoranjan Dey and my mom, Smt. Sabitri Dey for their unconditional support, love and encouragement.

Introduction

In biological systems, forces are essentially present at all levels, ranging from macroscopic to cellular, and even single molecule levels. Forces are implicated in growth and maintenance of muscles, bones, and blood vessels, regulation of blood pressure, movement of cells, regulation of cell multiplication, cell death and many other processes related to the lifecycle of a protein[1-5].

There are several current experimental methods for measuring forces and displacements in the single molecule level for proteins. The single-molecule spectroscopy methods are often classified into motion-sensitive techniques and force-sensitive techniques. The most well known motion-sensitive techniques are centroid tracking and Förster, or fluorescence, resonance energy transfer (FRET). The force-sensitive techniques are optical trap (OT), magnetic tweezers (MT) and force extension/force clamp atomic force microscopy (FX/FC-AFM).

The FX/FC-AFM relates closest to this thesis. The force-spectroscopy mode of a single molecule AFM can measure the forces acting on proteins and other bio-molecules while they are extended at local scales[6-13]. In the FX mode, a protein can be pulled at a constant velocity to achieve the force and extension required for unfolding it. In the FC mode the biomolecule is kept at constant pulling force and the extension of the biomolecule over the time of the experiment is observed. There are many examples of FX/FC force measurements of binding forces of complementary DNA strands[14], measurement of dissociation force between ligand-receptor systems[15], measurement of force responsible for conformational transitions in polysaccharides[16,17] and measurement of unfolding forces of multidomain proteins[18].

To apply the single molecule force spectroscopy (SMFS) with AFM one needs to use either a high quality commercial system, or a custom built set-up. High quality commercial AFMs include the Cypher[TM] AFM, from Asylum Research, Multimode from Veeco Metrology, ForceRobot300, from JPK Instruments, and Model# 5500 AFM, from Agilent. They all offer ~20-50 pm deflection noise in ~1 kHz bandwidth.

Our custom built single molecule AFM has ~100 pm of deflection noise at ~1kHz bandwidth and sub-nanometer of distance resolution. It was built and assembled using commercially available components. Having our own AFM gives us a chance to improve it with custom features. Another advantage is that it is far less expensive than the AFMs of similar capability. Personally, constructing the AFM gave me some hands-on experience with AFM.

This thesis is comprised of four chapters. Chapter 1 and chapter 2 are devoted to an introduction of AFM and construction of the single molecule FX/FC-AFM, respectively. Chapter 3 presents calibration and testing of this setup. Finally, Chapter 4 deals with application of this microscope into a concrete biological example, namely the pulling of a protein construct including Notch protein.

References:

1. J.A. Kenniston, R.T. Sauer, Signaling degradation. Nat. Struct. Mo. Biol. 11, 800-802 (2004)

2. A.W. Orr, B.P. Helmke, B.R. Blackman, M.A. Schwartz, Mechanisms of mechano transduction. Dev. Cell. 10, 11-20 (2006)

3. K. Svoboda, S.M. Block, Biological applications of optical forces. Annu. Rev. Biophys. Biom. 23, 247-285 (1994)

4. C.R. Hickenboth, J.S. Moore, S.R. White, N.R. Sottos, J. Baudry, S.R. Wilson, Biasing reaction pathways with mechanical force. Nature 446, 423-427 (2007)

5. C. Bustamante, Y.R. Chemla, N.R. Forde, D. Izhaky, Mechanical processes in biochemistry. Annu. Rev. Biochem. 73,705-748 (2004)

6. N.A. Burnham, R.J. Colton, Measuring the nanomechanical properties and surface forces of materials using an atomic force microscope. J. Vac. Sci. Technol. A 7, 2906-2913 (1989)

7. M.Reif, J. Pascual, M. Saraste, H.E. Gaub, Single molecule force spectroscopy of spectrin repeats: Low unfolding forces in helix bundles, J. Mol. Biol. 286, 553-561 (1999)

8. H.Dietz, M. Rief, Exploring the energy landscape of GFP by single-molecule mechanical experiments. PNAS USA, 101, 16192-16197 (2004)

9. Carrion M. Vazquez, A.F. Oberhauser, S. B. Fowler, P.E. Marszalek, S.E. Broedel, Jane Clarke and J.M. Fernandez, Mechanical and chemical unfolding of a single protein: A comparison, PNAS USA, 96, 3694-3699 (1999)

10. H.B.Li, W.A. Linke, A. F. Oberhauser, M. Carrion-Vazquez, J. G. Kerkvliet, H. Lu, P. E. Marszalek and J.M. Fernandez, Reverse engineering of the giant muscle protein titin, Nature, 418, 998-1002 (2002)

11. J.M. Fernandez, H.B. Li, Force-clamp spectroscopy monitors the folding trajectory of a single protein. Science, 303, 1674-1678, (2004)

12. P.E. Marszalek, H. Lu, H. Li, M. Carrion-Vazquez, A.F. Oberhauser, K. Schulten and J.M. Fernandez, Mechanical unfolding intermediates in titin modules, Nature, 402, 100-103 (1999)

13. M. Carrion-Vazquez, H. Li, H Lu, P.E. Marszalek, A.F. Oberhauser and J.M. Fernandez, The mechanical stability of ubiquitin is linkage dependent, Nat. Struct. Biol., 10, 738-743, (2003)

14. G.U. Lee, L.A. Chrisey, R.J. Colton, Direct measurement of the forces between complementary strands of DNA. Science 266, 771-773 (1994)

15. E.L. Florin, V.T. Moy, H.E. Gaub, Adhesion forces between individual ligand-receptor pairs. Science 264, 415-417 (1994)

16. M.Rief, F. Oesterhelt, B. Heymann, H.E. Gaub, Single molecule force spectroscopy on polysaccharides by atomic force microscopy. Science 275, 1295-1297 (1997)

17. P.E. Marszalek, H.B. Li, J.M. Fernandez, Fingerprinting polysaccharides with single-molecule atomic force microscopy. Nat. Biotechnol. 19, 258-262 (2001)

18. M. Rief, M. Gautel, F. Oesterhelt, J.M. Fernandez, H. E. Gaub, Reversible unfolding of individual titin immunoglobulin domains by AFM. Science 276, 1109-1112 (1997)

Chapter 1: Introduction to Atomic Force Microscopy

In this chapter, the reader is introduced with the Atomic force microscopy (AFM). General operating principles, imaging modes, and FX/FC experiments are described subsequently. Readers are introduced to main AFM components, namely AFM cantilevers, a position sensitive photo detector (PSPD) and a scanner. The chapter ends by listing the AFM limitations and most common artifacts.

1.1. A bit of history:

AFM belongs to the scanning probe microscopy methods. The forerunner of AFM was the scanning tunneling microscope (STM), which was built by Gerd Binnig and Heinrich Rohrer at IBM Research Institute in Zurich, Switzerland. G. Binning and H. Rohrer received Nobel Prize for Physics in 1986 for the development of STM. The first AFM was invented by G. Binning, C.F. Quate, and C. Gerber in 1986. AFM became commercially available in 1989.

1.2. General operating principle:

Figure 1.1 shows a schematic diagram of a standard AFM system. Typically AFM is used to obtain the topography of a given surface at sub-µm and µm length scales, i.e., to report what the surface looks like at these local scales.
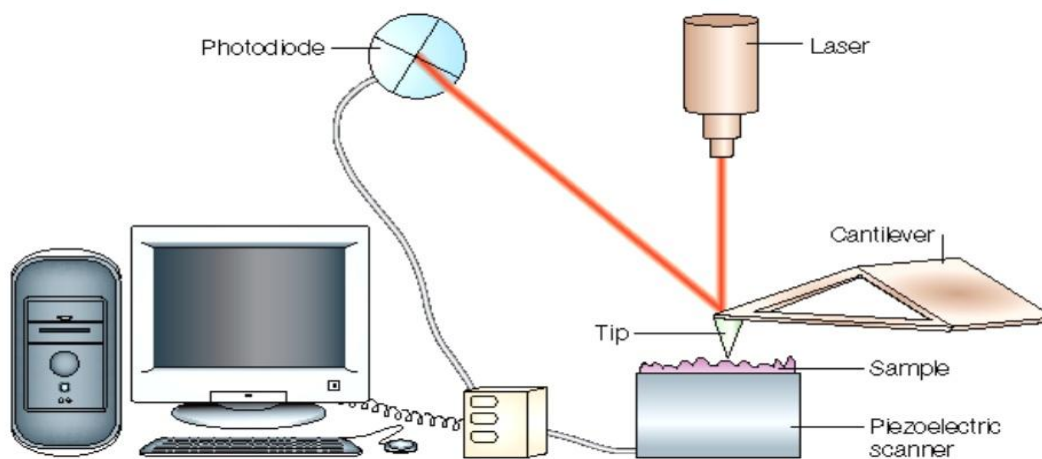
Fig 1.1 Principle of AFM: A laser beam is reflected from the upper side of the cantilever and goes to a photodetector. The deflection signal is a measure of force. The scanner movement in z direction is controlled by feedback electronics. In the constant force mode, the scanner provides a measure of the distance travelled. Scanners can be controlled by feedback electronics. In the constant force mode, the scanner movement in the z-direction gives the topography signal. The figure is adapted from www.geobacter.org

1.3. Imaging modes:

There are various AFM imaging modes. Each of them gives different information about the sample being imaged. Here I will discuss the most common types: (i) contact mode, (ii) non-contact mode, and (iii) tapping mode.

(i) The **contact imaging** mode is so named because the cantilever tip remains in contact with the sample at all times during scanning. This is the simplest mode. Typically, the sample resides on top of a piezo scanner. A laser beam is reflected from the upper side of the cantilever and goes to the PSPD. This arrangement is called "beam bounce detection system". The deflection signal is a measure of force. The scanner movement in z direction is controlled by feedback electronics. There are two variations of this mode: Constant force mode and constant height mode. As the name suggests, in the constant force mode, a feedback mechanism is utilized to keep the force on the cantilever constant. The scanner movement in the z-direction gives the topography signal. In the constant height mode, the feedback is turned "off", so that z-height remains constant, then the deflection signal is monitored to get a topographic image.

(ii) In the **non-contact (NC)** mode of imaging, the cantilever tip is held at ~ 5 to 100 nm above the sample surface. The cantilever is vibrated at a constant frequency, near its resonant frequency (typically between 50 to 400 kHz), with an amplitude in the order tens of nanometers. While the tip is scanned over the surface, the amplitude of cantilever vibration changes in response to force gradients which vary with the tip-to-sample distance. These changes in vibration amplitude yield the surface topography image. Alternatively, the amplitude of cantilever's vibrations is kept constant and the scanner either approaches or withdraws from the surface to keep the amplitude constant at a fixed frequency. Hence, in more common realization of this mode, NC imaging is very useful for imaging soft polymers and biomolecules. There is very little chance of the tip getting contaminated or damaged in this method.

(iii) The **Intermittent-contact (IC) or tapping** mode is very similar to the NC mode, except that in the IC mode, the vibrating cantilever touches the sample within its oscillation period. In the IC mode, the amplitude of cantilever vibration changes in response to force gradients which varies with sample-to-tip distance. Usually the changes in vibration amplitude relate to the surface topography image.

1.4. Force Extension (FX) and Force Clamp (FC) experiments

Apart from imaging, the AFM is often used to do force spectroscopy, i.e., to investigate the forces acting on the AFM tips as a function of either indentation or the tip-sample distance. The force-extension mode involves stretching the molecules clamped between the tip and the substrate at a constant speed. In the force clamp mode, a constant tensile force is applied to the molecule in question. More details about stretching proteins in these modes are explained below.

1.4.1. FX Experiments:
A typical FX trace for a polyprotein (fig.1.2 (A)) is shown in fig.1.2 (B). Typically, a drop of the physiological solution of a protein is deposited on the substrate. After the protein gets adsorbed into the surface, the AFM cantilever is used to pick, or to fish, the single protein molecules and stretch them. First, a cantilever tip indents the substrate. If a protein gets attached between the tip and the substrate, this point is typically defined as its zero extension of end-to-end length. Then, the cantilever is retracted from the substrate at constant speed.
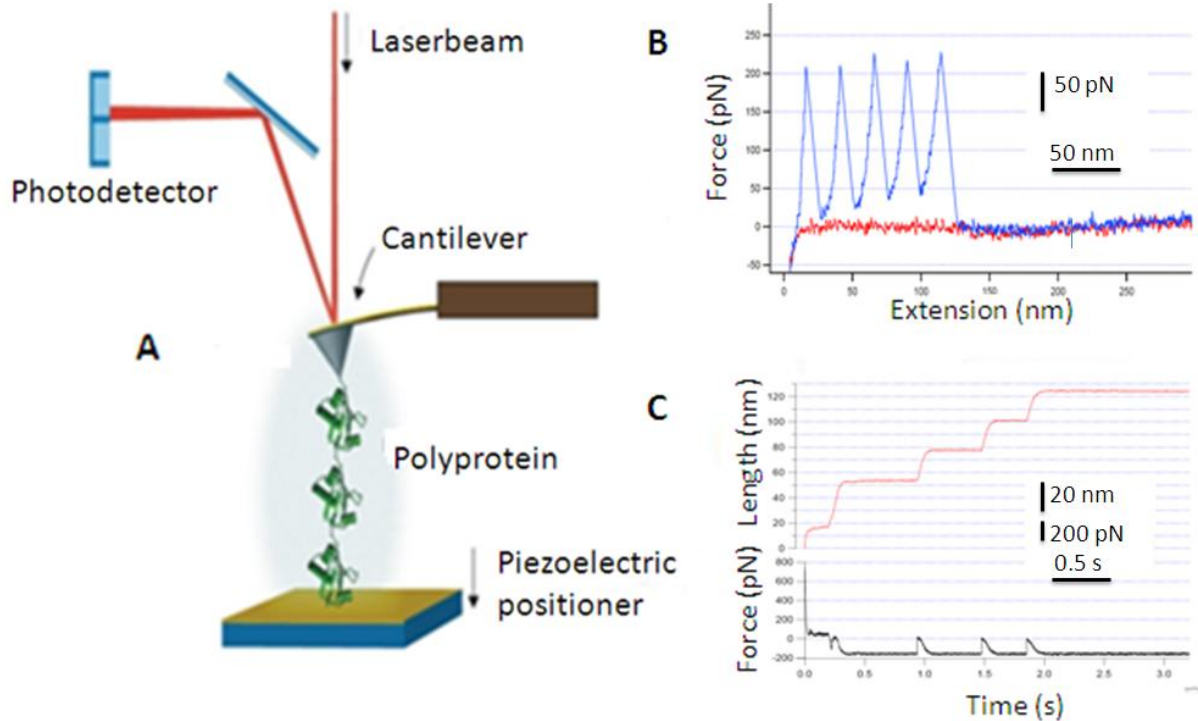
Fig 1.2 (A) A single molecule AFM is pulling a polyprotein. Typical FX trace (B) and FC trace (C) are shown.

The FX trace of a polyprotein has the distinctive feature of a saw-tooth pattern (fig 1.2 (B)). This pattern shows conformational transitions occurring during pulling of the protein. At first, entire molecule is stretched and the force increases to a peak value. At a force peak, the molecule is like a string of beads stretched to its maximum length. Next, there are two possibilities: either a unit of a protein untangles, or the sample-tip or sample-substrate contact breaks up. In the case of unfolding, the force drops to residual value for a moment as the cantilever relaxes due to extra length available. Next, the unfolded molecule gets extended again, hence the succession of events begins to repeat. The final peak on the saw-toothed pattern marks the loss of contact.

Usually, freshly cleaned glass or gold coated glass cover slips are the most efficient substrates[2]. Low protein concentration makes the probability of picking a single protein low, but enhances the probability of picking only one molecule at a time. The peak force on the FX experiment is a measure of the mechanical stability of a monomer of polyprotein and the extension yields the unfolding length.

1.4.2. FC Experiments:
The FX experiments cannot precisely measure force-dependent parameters. In the FC experiments, a protein is kept at a fixed stretching force and changes of the end-to-end length of the molecule are measured as a function of time (fig.2.1(C)). A significant conformational change, or an unfolding event of a protein, changes its end-to-end length. AFMs feedback compensates for such events by increasing the tip-substrate separation. The resulting AFM scanner motion produces a step on extension vs. time trace. Similar feedback action comes into play whenever the applied force is changed. Samples are prepared similarly as for an FX experiments.

3

1.4.3. Shortcomings of FX/FC-AFM spectroscopy:

The substrate-biomolecule and cantilever-biomolecule attachment points are not well defined. There is also a possibility of distorted data by the surface proximity, interaction with surface and knotting. Another shortcoming is due to a limited bandwidth (BW) of the FX/FC experiments. Currently, accessible time scales are from a millisecond to a hundred seconds, i.e. effective BW is in the range of hundredth of MHz to several kHz. As a result, some fast unfolding processes cannot be studied.

1.5. AFM Cantilevers:

There is a large range of AFM cantilevers available depending on applications. Most cantilevers are made of silicon or silicon nitride. Stiff levers are used to apply up to several nN of force, whereas, compliant levers are used to apply up to tens of pN of force.

Cantilevers are usually either rectangular or "V"-shaped. The sharp tip on the end of one side of a cantilever serves as a probe. Most of the probes look like either square base pyramids or cylindrical cones, although some more complicated shapes can be manufactured. This is typically done via electron beam lithography or ion beam lithography. Typical radii of curvature at the extremity of the tips are ~10 nm and typical lengths of a tip are ~20 μm.

Fig 1.3 Cantilevers. Adapted from www.mobot.org. The top surface of a cantilever (the surface opposite to the probe side) is often coated with a thin film of gold or aluminum to maximize the reflected light intensity.

1.6. PSPD:

In the most common "beam bounce detection system", any change in cantilever deflection produces a change in a position of the laser spot on the PSPD. Usually, a four-quadrant photodiode is used (see fig 1.4). Let A be the top left quadrant, B be the top right quadrant, C be the bottom left quadrant and D be the bottom right quadrant. Then, the vertical deflection signal is usually I(A+B) – I(C+D) and the lateral deflection signal is I(A+C) – I(B+D), where "I" stands for respective photo-currents produced by a photodiode.

1.7. Scanner:

Scanners of different shapes and sizes are available in the market. The most popular tube scanner is made up of a hollow cylinder of a piezoceramic material. The cylinder is expanded and contracted in the z-direction and bends in x and y direction by electric voltage applied to its respective sides. Upgraded types of scanners consist of separate piezocrystals for each direction of movement, or a stack of piezotubes. These arrangements have less imaging noise and less non-linearities than a tube scanner.

1.8. AFM limitations and its artifacts:

Although AFM is a very versatile system, it has few limitations like any other experimental set-up. The important AFM limitations are described in the following paragraphs.

1.8.1. Artifacts due to tip profile:

The common cause of artifacts in topography is the shape of the tip. Usually the shape of the tip is spherical, or paraboloidal, with the radii of curvature between 10nm and 100nm. This is significant when dealing with surface roughness of similar size. The length of certain feature may turn out to be larger by geometrical arguments because of convolution with the tip profile. The shape of the tip can also change frequently due to wear. Also, while doing the scanning, the tip can pick up some surface adsorbents. Poorly manufactured tips are another source problems. This includes double, tilted, and non-centered tips. For example, if the tip is not centered with respect to the cantilever's longitudinal symmetry line, varied torque is produced in forward and reverse scans, and the friction loop (see appendix B) becomes asymmetrical. One way to check the tip profile is to use a calibration grating from which the tip profile could be de-convoluted.

1.8.2. Artifacts due to feedback:

Some artifacts come from contact mode imaging with constant force. The feedback electronics strive to keep the force constant throughout scanning. But a local change in elasticity and adhesion of the sample at the surface acts as an extra attraction or repulsion. These produce incorrect topography imaging.

1.8.3. X-Y-Z Couplings:

Couplings between X-Y-Z directions in a cantilever and a scanner are described as follows (see fig 1.4). First, only one end of the cantilever is clamped to the cantilever holder. Hence, the tip movements are parabolic rather than linear and any displacement in one axis is coupled to the other two axes. Next, a typical AFM scanner is a tube. Although the displacement in z-direction is controlled by a feedback mechanism, the displacements in X induce additional displacements in other axes. Next, the cantilever is tilted with respect to the plane of the sample surface. This is necessary so that the tip of the cantilever touches the surface first. Because of this tilt, however, vertical displacements of the cantilever holder, or scanner, introduce some additional lateral displacements
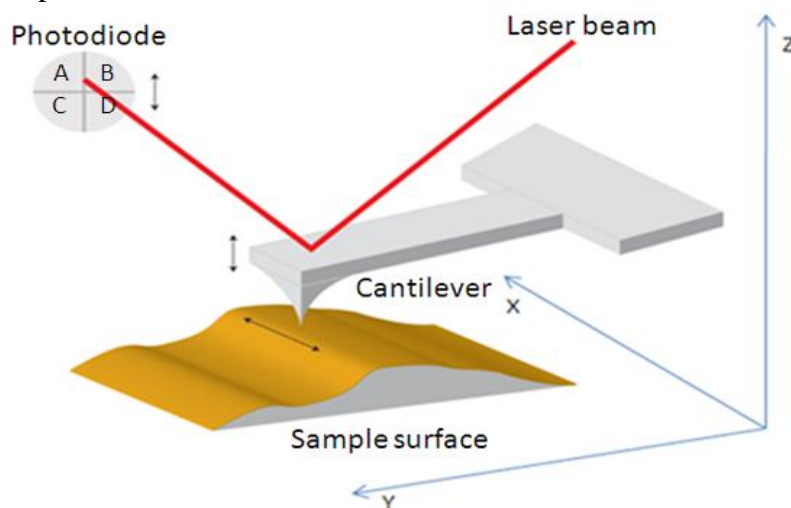
Fig 1.4 The figure presents a typical set-up while an AFM scanning the surface in X-Y and detecting topographies in z-direction. Partially adapted from www.scienceinyoureyes.com

1.8.4. The issue of noise:

Three types of noise are encountered in AFM measurements: mechanical, thermal and electronic.

Mechanical Isolation: Mechanical isolation describes how well a given AFM system is decoupled from outside mechanical and acoustical vibrations. An anti-vibration system table, or an acoustical isolation, or suspending an AFM can help to decrease mechanical noise. Also, any cables lying on the anti-vibration table should not be too stiff. This would limit any transfer of mechanical vibrations.

Thermal Stability: While working with atoms, thermal stability is an important concern. Even a change of 1K can expand a 1 cm block of steel by ~100 nm. Mechanical dimension of the AFM should be minimized to lower this expansion. The AFM scanner becomes heated by applied high voltage of about several hundreds of volts. Therefore, it is recommended to turn on the scanner about 30 minutes before the initiation of the experiments.

Stability of Electronics: The electronics can add additional noise, mostly electromagnetic in nature. Electronic instruments can also impair the quality of experimental data by affecting feedback electronics.

References:

1. A. del Rio, R. Perez-Jimenez, R. Liu, Pere Roca-Cusachs, J.M. Fernandez and M.P. Sheetz, Stretching single talin rod molecules activates vinculin binding, Science, vol.323, pp 638-641 (2009)
2. M. Carrion-Vazquez, A.F. Oberhauser, S.B. Fowler, P.E. Marszalek, S.E. Broedel, J. Clarke and J.M. Fernandez, Mechanical and chemical unfolding of a single protein: A comparison, PNAS USA, vol 96, pp 3694-3699 (1999).

Chapter 2: Construction and operation of the single molecule FX/FC-AFM

The single molecule AFM was constructed from commercially available components as well as custom built parts. This chapter starts with a description of its construction and the main parts used. Finally, a brief operational manual is provided for future users.
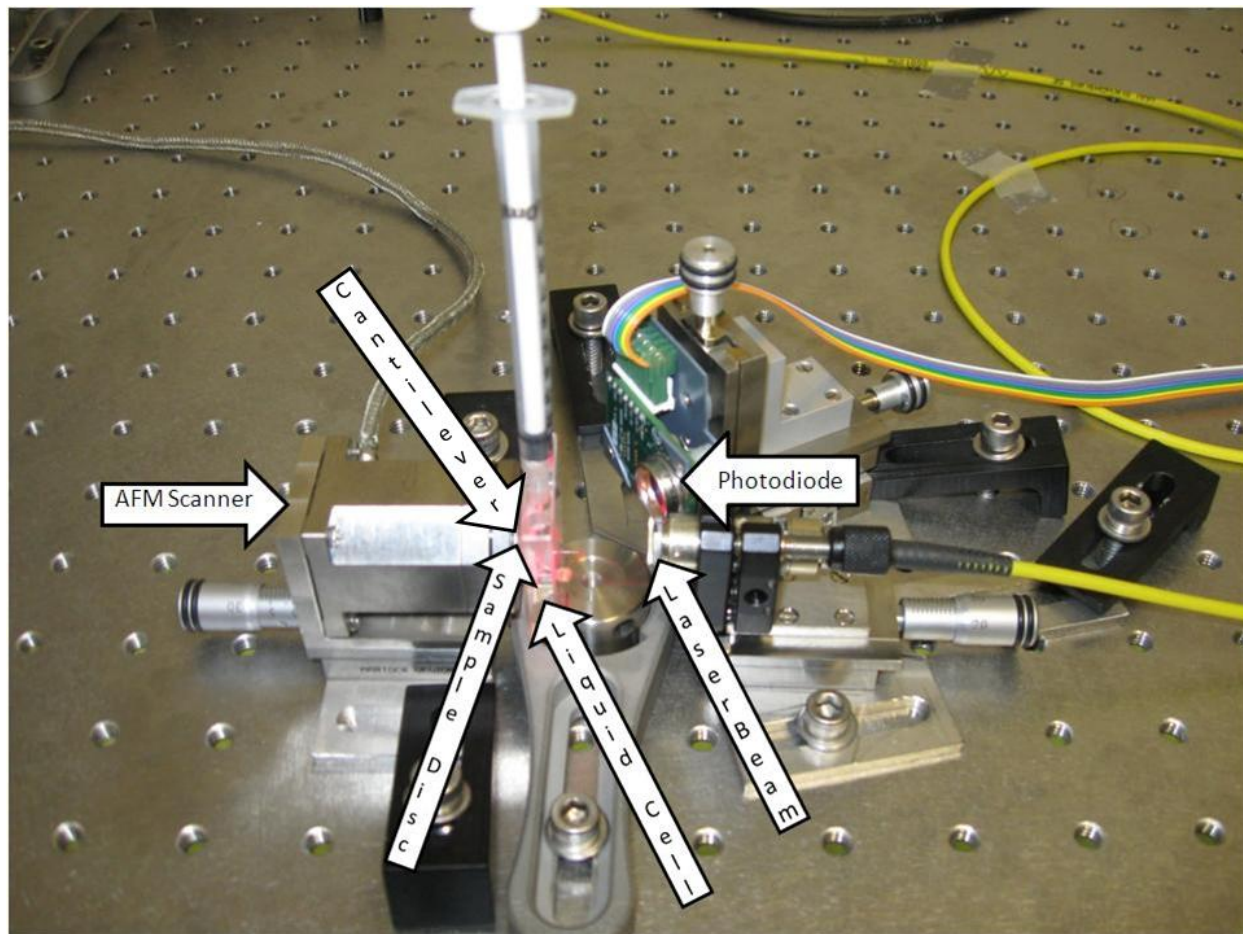
Fig 2.1 The picture shows a part of our single molecule AFM.

2.1. Principles for connecting electronics parts:

The feedback and data acquisition devices consist of Simple Instrumentation Modules (SIMs) from Stanford Research Systems (SRS) and the data acquisition cards (DAQs) from National instruments (NI). The (A+B) signal from the photodiode is directly acquired by the DAQ devices. The (A-B) signal from the photodiode is processed first by the SIMs and then acquired by DAQ devices. Similarly, the Z-piezo output signal is processed by the SIMs and then enters the DAQ devices. Scanner's X and Y-control input/output signals come from DAQ devices.
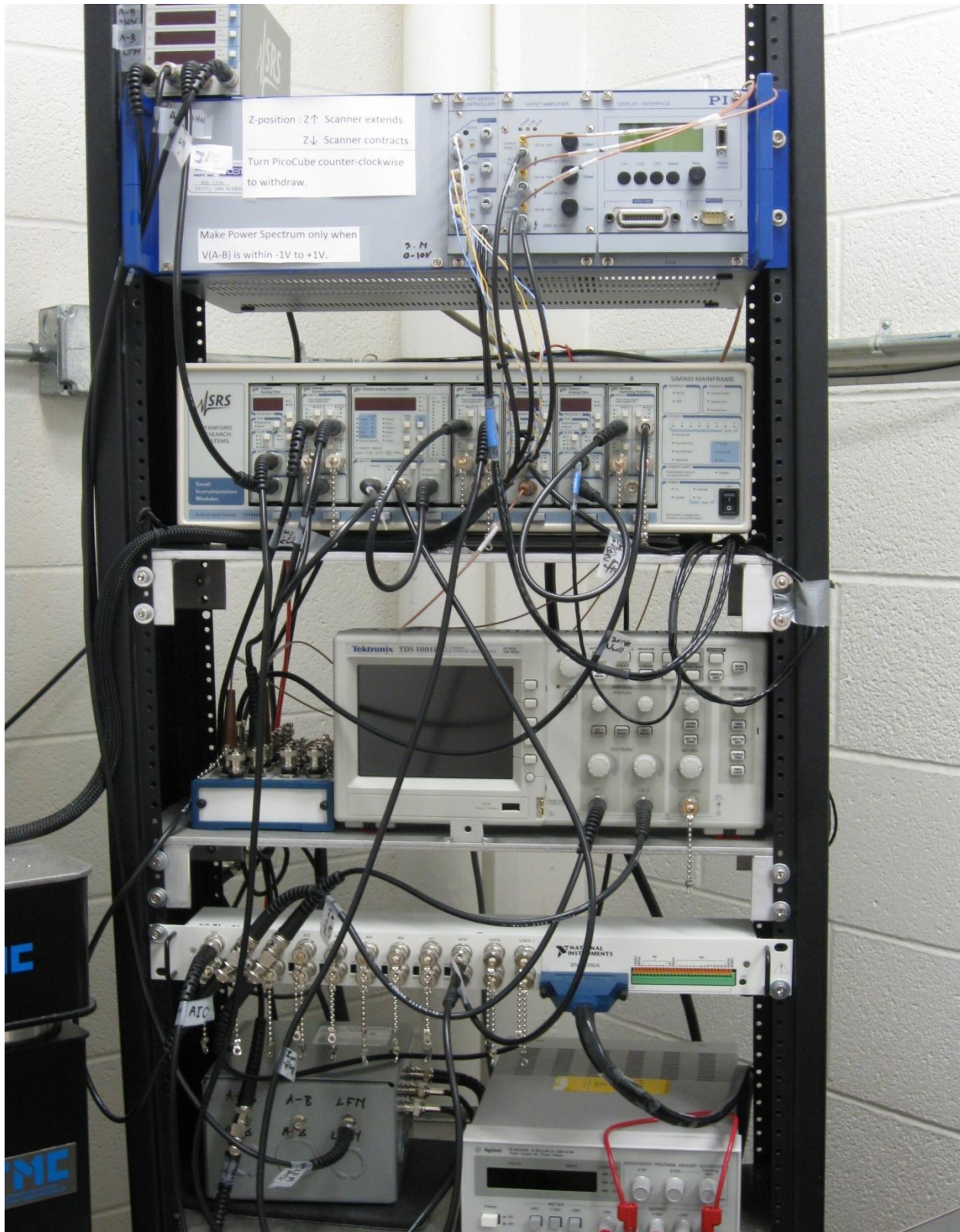
Fig 2.2 The AFM electronics (scanner controller, feedback electronics, DAQs etc.)

2.2. Software:

The software for running the AFM was developed in IGOR, a software for scientific programming from Wavemetrics, USA. It was partially developed by Prof. Fernandez's group at Columbia University and partially by our team. A special package, NIDAQ tools, available from Wavemetrics, was responsible for transferring the commands from the software to the DAQ devices. Also, GPIB commands provided commands to the SRS SIM modules which were connected to computer through a GPIB cable. Another program written in IGOR was used for analysis and treatment of the experimental data.

2.3. Description of the constituent parts of the AFM:

The single molecule AFM was built using the following components:

A. SIMs from SRS:

The SIMs were used for processing the electrical signals from a PSPD and a scanner. These were (a) Mainframe (SIM 900), (b) Analog Filters (SIM965), (c) Summing Amplifiers (SIM 980), (d) Analog PID Controller (SIM960) and (e) Quad digital voltmeter (SIM970).

(a) SIM900 is a mainframe in which up to 8 SIMs can be plugged in. There is provision for a 9th module connection through an interconnect cable outside the mainframe which was used here. There is an option for computer operation, used in our set-up, along with a front panel operation. The Mainframe supplies power, interfaces with the computer, clock synchronization, and the status of individual modules. The mainframe was connected to the computer with a GPIB (IEEE-488.2) connection. All commands to the individual SIMs are sent through the mainframe interface.

Fig 2.3 The Mainframe (SIM900). Adapted from www.thinksrs.com

(b) Analog Filters (SIM965) were used for signal conditioning applications. It has a low/high pass option for Bessel and Butterworth filters. Bessel filter gives sharp step response, very low overshoot, and linear phase response. Butterworth filter gives good pass-band flatness with some overshoot. Like all other SIMs, SIM965 is fully programmable. Here we used Bessel filter in a low pass mode.

(c) Summing Amplifier (SIM980) has 4 input channels. These channels can be used to add or subtract signals from each other. It is very useful in many analog applications in our single molecule AFM.

9

Fig 2.4 (A) Analog filter (SIM965), (B) Summing Amplifier (SIM980), (C) Analog PID controller (SIM960) and (D) Quad DVM (SIM970). Adapted from www.thinksrs.com

(d) Analog PID controller (SIM960) was used for controlling the AFM feedback. The controller parameters, i.e., proportional, integral, and differential gain (P,I,D) values can be changed and monitored via front-panel controls.

(e) Quad DVM (SIM970) was used for a visual display of the key AFM signals, i.e., the total intensity of light on a photodiode or a deflection signal (a measure of force).

B. DAQs and BNC boxes from NI:

Our AFM uses two National Instruments' Data Acquisition Cards, NI PCI-6281 and NI PCI-6733. Their output channels controlled the scanner. Their input channels acquired vital AFM signals. NI PCI-6281 has a data acquiring speed of 500 kS/s (kilo-Sample/sec) in multichannel and 625 kS/s in single-channel mode. It has 16 analog inputs of 18-bit resolution, but only 2 analog outputs of 16 bit resolution. NI PCI-6733 is a 16 bit-resolution card with high speed analog output of 1 MS/s, 16 bit of resolution, and 8 digital I/O channels. These cards has +/-10 volts input/output signals. The shielded BNC boxes interfaced communication between the DAQs and AFM electronics (SIMs and PI controller). BNC-2090A and BNC-2110 were used with PCI-6281 and PCI-6733, respectively.
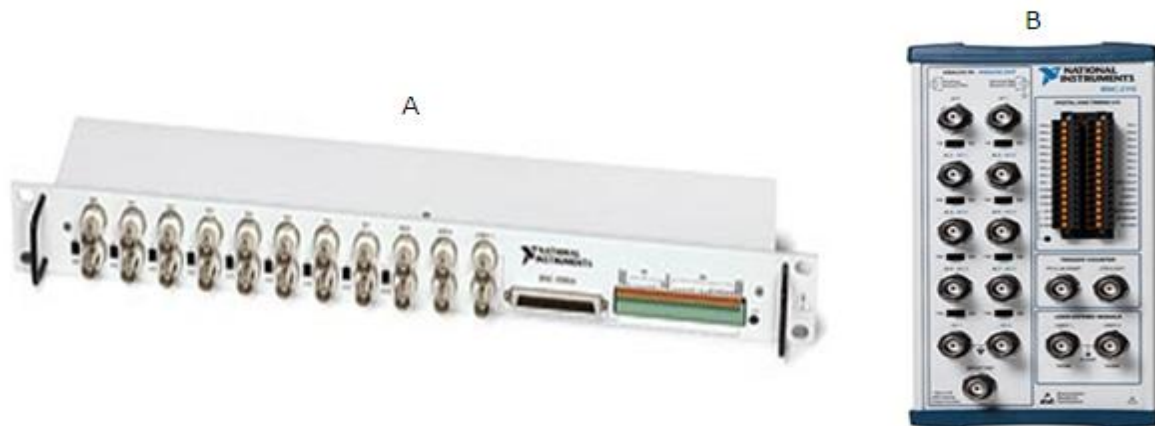
Fig 2.5 (A) BNC-2090A and (B) BNC-2110. Adapted from www.ni.com

C. Scanner (PZT) and Scanner controller from Physik Instrumente:

P-363 Pico-Cube, a XYZ PZT from Physik Instrumente (PI) GmbH & Co., Germany was used in our single molecule AFM. It can travel 5 μm in all X, Y and Z directions and has a resolution of 50 pm in the Z. It can work in an open and closed loop configuration. Open loop is defined as when the internal scanner feedback, servo unit, is off. Closed loop is defined as when the feedback servo unit is on. It is one of world's fastest and highest precision XYZ PZT for AFM. It is composed of a stack of piezos with low hysteresis and creep. Its resonant frequency is 9.8 kHz in the Z. The resonant frequency in X,Y diminishes to half of unloaded resonant frequency for 20 g of load on the scanner. To minimize the mechanical load, we used the Pico-Cube in a horizontal configuration. An important feature of this PZT is the high-resolution capacitive sensors for true sensing of the scanner displacement with 0.1 nm resolution. We have used the PZT in an open-loop configuration, i.e. with no internal feedback. The PZT controller intended to control P-363 PicoCube system is the controller from PI, E-536. It provides voltage control of a pico-cube in a closed and open loop, and reads out the signals from the position sensors.
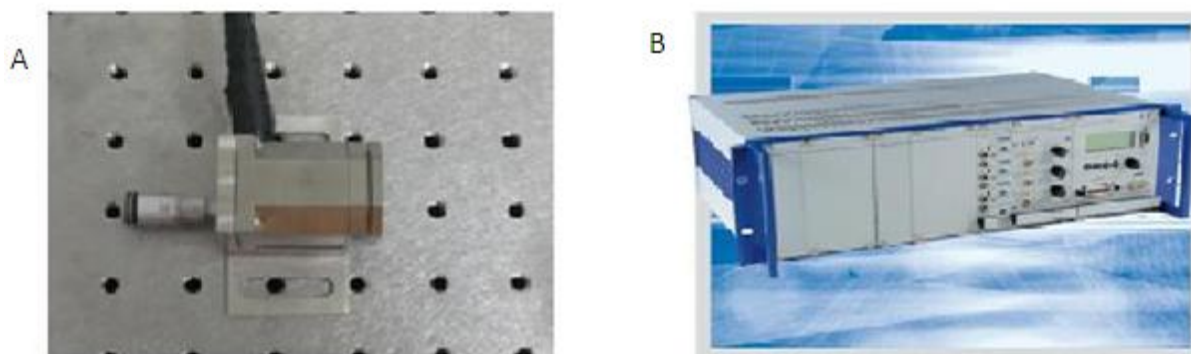
Fig 2.6 (A) Piezo-scanner P-363 (Pico-Cube) and (B) Scanner controller E-536 from Physik Instrumente, Germany. The 2nd picture is adapted from www.physikinstrumente.com

D. PSPD from Pacific Silicon Sensor:

The PSPD used in this AFM is model # QP50-6-18u-SD2 from Pacific Silicon Sensor. It is a quad photodiode array with low noise current-to-voltage amplifiers. It yields lateral and vertical deflection signals as well as total intensity signal. The PSPD was mounted on a 3-axis translation stage from Elliot Scientific, UK.

Fig 2.7 Position sensitive photodiode. Adapted from www.pacific-sensor.com

E. PSPD normalizing board (NORM) circuit and NORM box:

The NORM circuit normalizes the vertical and lateral deflection signals by dividing them by the total intensity. Normalization is important because light intensity can fluctuate over time. The circuit is based on a wide bandwidth analog multiplier MPY634 with a bandwidth of 10 MHz.

The circuit diagram is shown in Fig 2.11. The output in the diagram is $\propto \dfrac{(A-B)}{(A+B)}$.
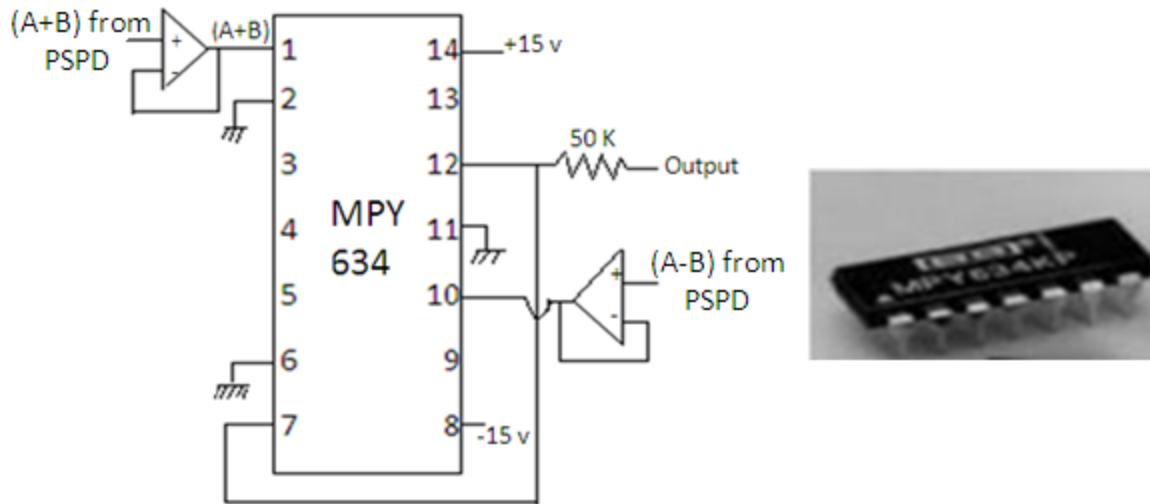
Fig 2.8 Circuit diagram of NORM circuit and picture of MPY-634 Analog multiplier.

The **NORM box** was custom built to house the NORM circuit, to supply power to PSPD, and to get (A+B), (A-B)Norm and LFM output signals. A standard metal electrical box of dimensions of 6in X 6in X 4.5in was chosen for this purpose so that no external electromagnetic wave could affect it. The BNC female connectors were fixed on the box. The input and output signals were taken through BNC cables. Care was taken to avoid common ground parasitic currents.
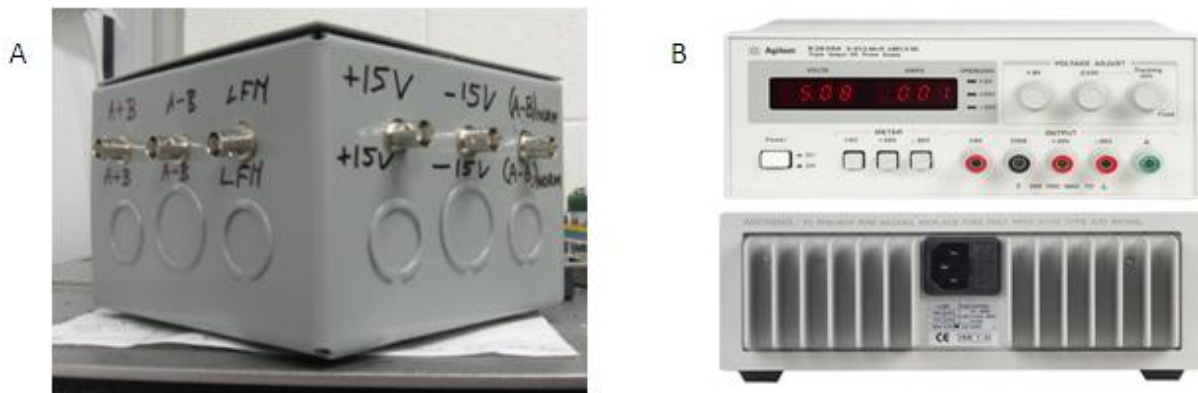
Fig 2.9 (A) The NORM Box and (B) DC power supply E-3630A from Agilent. (B) is adapted from www.agilent.com

F. Photo-diode and NORM power supply from Agilent Technologies:

DC power supply E-3630A from Agilent was used for powering the photo-diode circuit with +/- 15 V. The E-3630A has triple power outputs for bench top applications. Maximum power for

this power supply is 35 W. The peak-to-peak noise is 1.5 mV and normal mode rms voltage is 350 μV in the bandwidth of 20 Hz – 20 MHz. The current and voltage resolution is 10 mA, and 10 mV, respectively. Typical currents drawn by PSPD were 10-12 mA.

G. Laser from Schaefter+Kirchhoff:

The laser was a 6 mW diode laser, "51nanoFCM-660", from Schaefter+Kirchhoff, Germany. It has reduced power noise and low speckle contrast. This laser source has a reduced coherence length and a tight beam diameter which help to avoid interference. The coherence length is 300 μm, noise is less than 0.1% RMS, and its output power is changeable using potentiometer, or the voltage controlling input. Besides, it has a single-mode fiber cable and FC-APC (fiber cable - angled physical contact) connector at 8° polish. This 8° polish minimizes the intensity of reflected beam going back to the laser. The collimator "60FC-4-M20-10" from Schaefter+Kirchhoff produces a spot of less than 20 μm in diameter at a focal length of 20 mm.
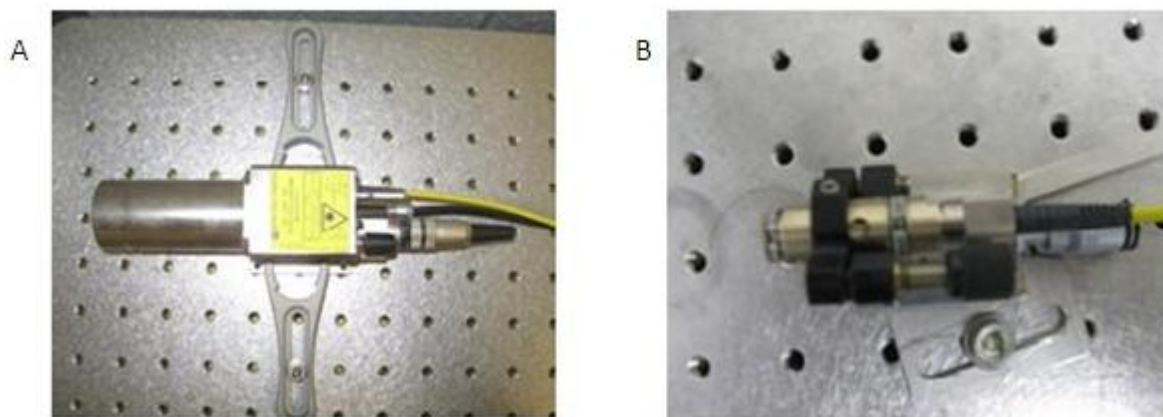
Fig 2.10 (A) Laser diode "51nanoFCM-660" and (B) collimator "60FC-4-M20-10" from Schaefter+Kirchhoff Germany. The collimator was mounted on a two axes tilt stage (KM05 from Thorlabs) which was mounted on one-axis translational stage from Elliot Scientific.

H. Vibration isolation laboratory table:

A pneumatic table with an optical top (model# 63-533), from Technical Manufacturing Corporation (TMC), was used to damp mechanical vibrations and to mount the AFM components. Isolation efficiencies at 10 Hz are 90-97% for both vertical and horizontal directions.

I. Liquid cell (LC):

A liquid cell from a Multimode AFM (Veeco metrology) was used in our set-up. It was glued permanently on a 0.75" high Newfocus pillar using epoxy adhesive.
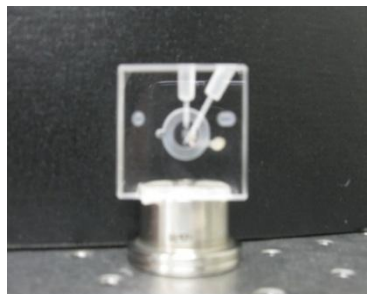
Fig 2.11 Liquid cell used in our AFM.

J. Mechanical adapter plates/pillars:
The clamps and screws were bought from Thorlabs. The pillar was purchased from Newfocus and the micropositioners (precision is 10 μm) were purchased from Elliot scientific. The adapter plate was designed by us and machined at Kansas State University.

2.4. Operating instructions for the single molecule AFM

The following paragraphs are step by step operating instructions for the single molecule AFM.

2.4.1. Turning on the AFM instruments:
(i) Turn on the Laser.
(ii) Turn on the PI Pico-Cube (Piezoelectric Transducer).
(iii) Turn on the SIM900 Mainframe.
(iv) Turn on the Oscilloscope (if necessary).
(v) Turn on the PSPD Power Supply.
(vi) Just before starting the experiment, float the anti-vibrational table by turning on the N_2 gas.

2.4.2. AFM experimental set up procedure:
Clamp the laser on the optical table at a distance of about a focal length (~ 20 mm) from the liquid cell (See fig 2.1). After putting the cantilever on the liquid cell, place that in front of the laser beam with a lever to beam angle of ~ 90 degrees.

A. Laser alignment: Look at the shadow image of the cantilever on the white paper screen. Now, approach/retract the laser via turning the micrometer screw. The image will get bigger or smaller. Turn the micrometer screw in such a way as to increase the size of an image. If you keep going that way, at certain point you will see the image disappears and if you keep on going further, you will see the inverted image of the cantilever. This happens because of simple principle in geometrical optics that you get inverted image once you cross the position of the focal length.

      Now, move back to the position in the middle between the upright image and the inverted image. Typically you will see that most of the laser beam gets reflected and little intensity is transmitted. In other words, you will see a circle with very low intensity on the white paper screen. This is good since it means that the laser spot is tightly focused on a cantilever. Now put a paper card on the position where you are supposed to place the photodiode. Try to get the reflected beam as circular as you can without any cross or interference rings (like that of Newton's rings). The cross on the reflected beam is an indication that the laser beam is at the very tip of the cantilever. One line of light superimposed on the reflected circular beam is an indication that the incident laser beam is on one of the "legs" of the cantilever.

      Now, bring the PSPD so that the reflected laser light falls on the active area of the PSPD quadrants. Next, using a paper card, align the position of the PSPD so that the reflected laser beam is perpendicular to PSPD's active area. Again, optimize the reflected beam to be as circular as possible and make sure that no interference ring is there. To achieve this, a little touch on the two screws of the laser holder may be enough. Move the PSPD's micropositioners so that both the vertical and horizontal deflection signals are near to zero. At this point, the alignment of the laser beam is complete.

B. Sample holder preparation: Typically, the sample holder consists of a 15 mm diameter metal disc and a glass cover slip glued together with one "Lift-n-press adhesive tabs" from Tedpella, USA. During gluing, you should be cautious not to handle the glass cover slip in too many places.

C. Sample preparation: The sample is a protein solution with an appropriate buffer (e.g. PBS or Hepes). Typically, you have to use a pipette to drop the prescribed amount (typically 20-30μl) of the sample on the glass cover slip side of the sample holder. Try to spread the sample using the tip of the pipette. While doing so, be careful not to touch the glass cover slip with the tip of the pipette because it may scratch the glass. Give it some time to dry, 20-30 minutes may be enough for drying, but that will really depend on the concentration and other properties of the sample. If the sample takes a long time to dry up, it may be a good idea to cover it using a glass petri-dish to protect it from dust.

D. Sample mounting on a PZT: Now, put the prepared sample holder on the face of the PZT having a small magnet. Care should be taken not to put any mark of grease or other contaminant from hand on the surface of the PZT. To achieve this you can use latex gloves, or tweezers. The center of the sample holder should come nearly to the cantilever when approached.

E. PZT Clamping: Now clamp the PZT parallel to the liquid cell, estimating with the naked eye. Care should be taken not to be very near to the cantilever to begin, otherwise, the cantilever may break.

F. Injecting the buffer: Use about 0.2-0.4 ml of an appropriate buffer (the one used for a protein solution) into a syringe, typically a 1 ml syringe. Get rid of any air bubbles by shaking the syringe, and fix it on the top-center hole of the liquid cell. Form a liquid meniscus between the liquid cell and sample. Care should be taken to make only one meniscus with no air bubble in the inner circular region. It is important not to add too much buffer to protect the PZT. PZT operates at -250 to 250 volts, so any liquid penetrating inside the PZT can cause irreversible damage.

G. Floating the anti-vibrational table: Turn on the N_2 gas to float the anti-vibration table.

H. Software initialization: Now open the RunAFM procedure in IGOR. Run the macro "Initialize SRS for FX" to perform the force extension experiment (FX), or "Initialize SRS for FC" to perform the force clamp experiment (FC). Then run the macro "Initialize DAQ" to initialize the Data acquisition devices. Now, go to the AFM panel and click on "Experiment Info" tab. After you choose the "Ultrafast AFM" in the "Setup", the whole "The AFM" window will be active.

I. Initial check-ups: At this point, take few FX curves by pressing GetFX button after pressing HeadNull button. FX trace consists of plotting the force vs. extension. The trace (going to the sample) and retrace (withdrawing from the sample) should overlay on top of each other. If they do not overlay, wait for the system's thermal drift to decrease (15-30 minutes). After thermal stabilization, check for interference. Interference shows up as sinusoidal force curves.
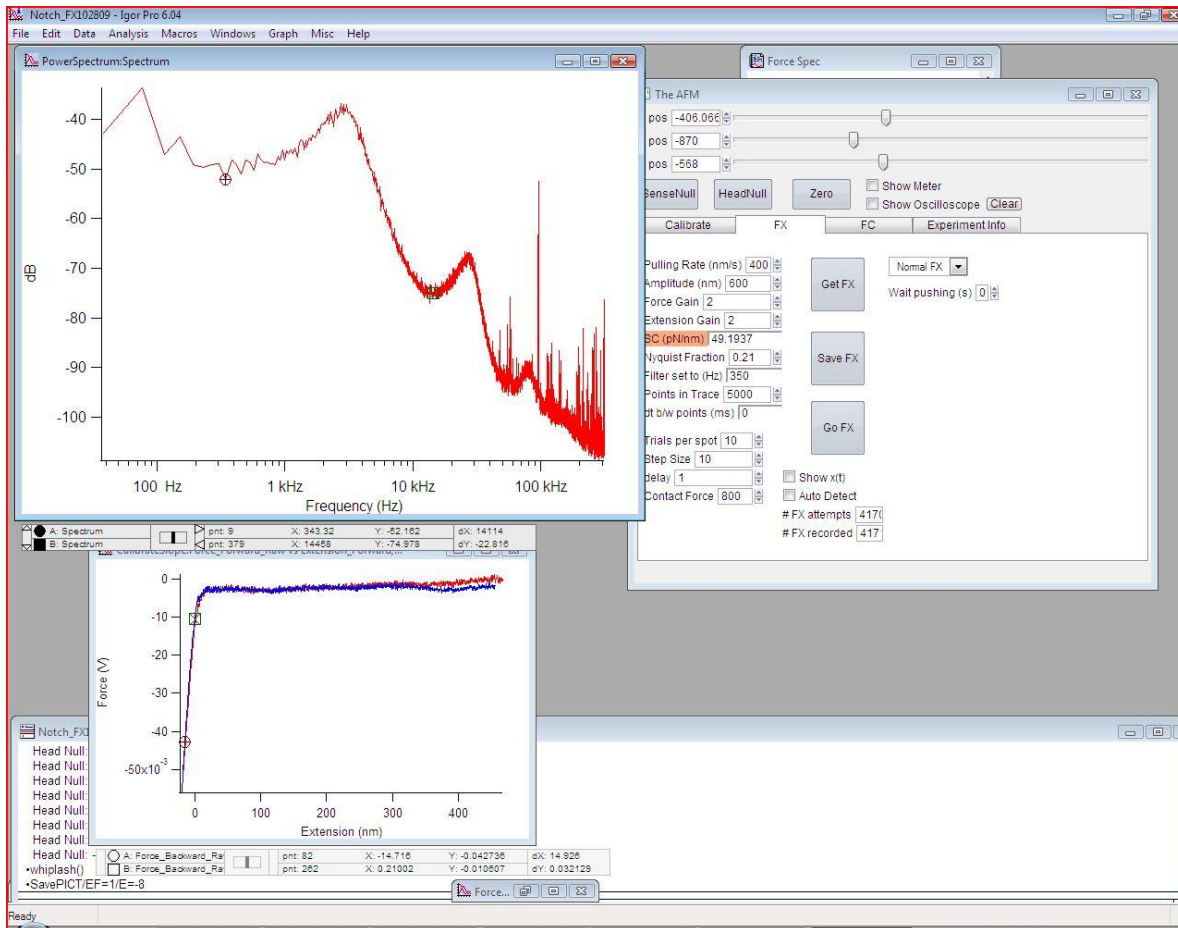
Fig 2.12 Screenshot of the computer screen during the start of experiment.

Now go to the "Calibrate" tab. Typical values are Pulling Rate (nm/s) is 400; Amplitude (nm) is 600; Force Gain is 2; Extension Gain is 2; # Averages is 124; Spectrum # points= 2^{14}.
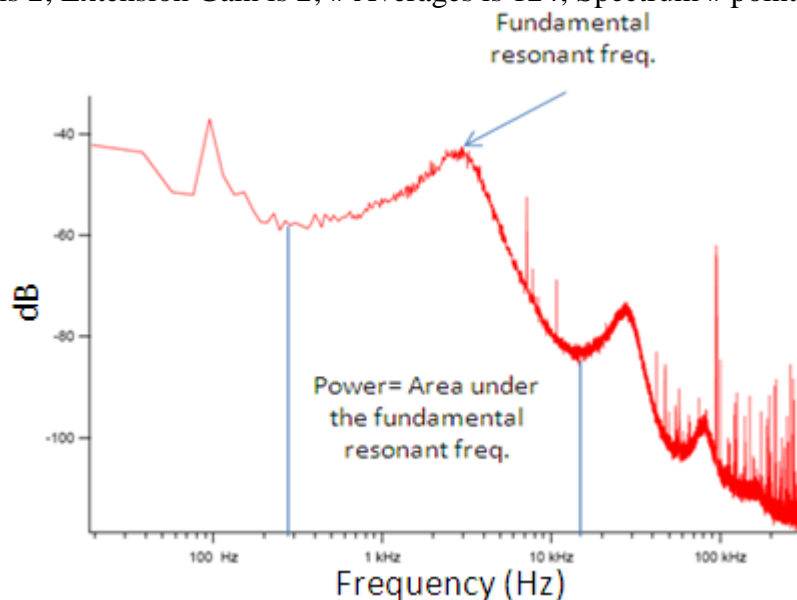
Fig 2.13 Power spectrum of MLCT type-D lever in liquid for cantilever's spring constant calibration.

J. Power Spectrum: Now click on the "Power" button and view the power spectrum.

(i) Note the cantilever's resonant frequency. Look at the box containing the cantilever you used. It should contain information about the first resonance mode of the particular cantilever you are using. A Veeco MLCT cantilever chip will have A,B,C,D,E and F type cantilevers and their corresponding resonant frequencies in the air are written on the box. In liquids, the resonant frequency diminishes. For example, Veeco MLCT type D lever has resonant frequency of ~ 12 kHz in air and ~ 3 kHz in liquid.

(ii) The dY difference between peak of the Power spectrum and the lowest point after the peak is called the Signal to Noise ratio (S/N). A typical value is about 45-60 dB. As the name suggests, the bigger the S/N ratio is, the better it is.

(iii) Now put the cursors in the two points in the Power spectrum which contain the resonance frequency peak in between. Look at the power (A-B_Vrms^2) in the window. Power (A-B_Vrms^2) should be in the order of 10^{-6} in water/buffer and 10^{-7} in air for V(A+B)= 9.5 V. Try to achieve the maximum value for power. To do this, you may have to take few power spectrums. Remember to adjust (A-B)Norm ~ 0 V and LFM ~ 0 V before taking any power spectrum. In fact, the (A-B)Norm cannot exceed 1 V.

**K. Approach to contact:** Now bring the PZT very near to the cantilever by clockwise movement of the PZT micrometer screw. Be extremely careful. Otherwise, you may break the cantilever. While turning the micrometer screw clockwise, keep your eye on the (A-B)Norm voltage on the SRS SIM970 Quad Digital Voltmeter. If the (A-B)Norm voltage becomes suddenly high, that's an indication that the PZT is in contact with the cantilever. Now, move a very short distance backward by turning the micrometer screw counter-clockwise. The next thing will be to go to "The AFM panel" in the software and increase the value on the "Z pos" until you see that the magnitude of (A-B)Norm has increased noticeably. Increasing the value of Z pos expands the PZT so that it touches the cantilever. At this point, you have to do a slope curve.

L. Contact Slope (for cantilever's spring constant calibration): Click on the "FX" tab and click the "HeadNull" and "SenseNull" buttons. After that, click on the "GetFX" button. A typical slope calibration curve in Force (V) vs. Extension (nm) looks like fig 2.15. In the contact region, the Slope is calculated from this curve in nm/V. Spring Constant (SC) in pN/nm is calculated from Power and Slope as described in the section 3.2. Typical values of slope are about 220-250 nm/V and the spring constant should be around 50 pN/nm for the Veeco MLCT type D lever. For MLCT type C lever, the spring constant should be 20-25 pN/nm.
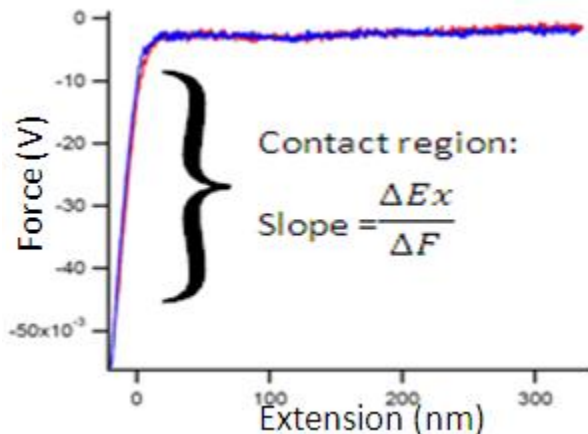
Fig. 2.14 The FX trace for calculating the slope. Veeco MLCT type D cantilever was used.

M. FX Experiment : You can click the GoFX button and start the experiment.
Typical values in the FX tab are:
Nyquist Fraction: 0.2
Points in trace: 5000
Trials per spot: 10
Contact force: 800-1200 pN
If you "check off" the "Auto Detect", the program will store only the graphs which meet the specified criteria in the program. After the experiment is over, save it. The graphs are now saved in Data Browser. You can go to Data Browser by clicking Data→ Data Browser in the window. To see and analyze the graphs, use the program "AFM_Analysis".

N. FC Experiment: To do the FC experiment, you can click the GoFC button and start the FC experiment. Typical values in the FC tab are:
Contact force: 800 pN
Contact time: 1 sec
Force gain: 2
Extension gain: 2
Nyquist fraction: 0.41
Points in trace: 60000
Trials per spot: 10
Pull force: -150 pN
Relax force: -20 pN
Pull duration: 5 sec.
Just like the FX experiment, after the experiment is over, save it. The graphs are now saved in Data Browser. You can go to Data Browser by clicking Data→ Data Browser in the window.
To see and analyze the graphs, use the program "AFM_Analysis".

2.4.3.Turning off the single molecule AFM equipments:
(i) Turn off the Laser.
(ii) Turn off the PI Pico-Cube.
(iii) Turn off the SRS SIMs.
(iv) Turn off the Oscilloscope (if used).
(v) Turn off the Power Supply of Quadrant Photo-diode (PSPD).
(vi) Turn off the N_2 gas knob.

2.5. Miscellaneous procedures:

2.5.1. NIDAQ self-calibration procedure:
From time to time, you will need to calibrate the DAQs to remove any offsets. To do so, click on to the "Measurement & Automation Explorer" icon on the desktop. Then, under the "Configuration" panel, click on "Devices and Interfaces". Now, click on the "NI-DAQmx Devices", and then right-click on "NI PCI-6733:Dev2" and click on "Self-Calibrate". Once the "Self-Calibrate" window appears, follow the instructions. To do the Self-calibration on "NI PCI-6281:Dev1", you will need to disconnect the cable to the BNC box (BNC-2090A) and then right-click on "NI PCI-6281:"Dev1". Click on "Self-Calibrate" and follow the on-screen instructions.

2.5.2. PicoCube cleaning procedure:
At the end of an experiment, watch for any liquid on the surface of the PicoCube. If there is a liquid spot on it, you will have to clean the PicoCube. Use a small quantity of isopropanol on a lint-less paper or a paper towel and clean it carefully. Never press against the surface of the PicoCube and be as gentle as you can. Then repeat using a very small amount of water on a towel. You might have to do this procedure several times before the mark goes away. Never allow any water drop to penetrate the PicoCube.

2.5.3. Metal disc and glass cover-slip gluing technique:
If you watch carefully, the metal discs (15 mm dia) from Ted Pella have one side flatter than the other. We want to have the flatter side towards the PicoCube's magnet. So, glue the other side (which has a little curvature) to the glass cover slip.

2.5.4. Evaporation procedure:
Often the substrate surface is a gold evaporated glass slide. Typically we deposit 15 nm of Cr to bind gold and then 50nm of Au on the glass cover-slip. For evaporation, we used VARIAN Vacuum Evaporator Model VE10. Au and Cr were purchased from Kurt J Lesker. One piece of Cr and 2 cm of Au is used at one time. The tungsten basket was purchased from Ernest F Fullam. On the top panel of the Evaporator, there is:
- Pressure gauge (typically kept at 0.01 torr range);
- AC micro-ammeter;
- Three switches for vacuum operation; OPERATE, CHANGE and STOP;
- A knob to display the operating range of vacuum pressure;
- A current knob;
- Manipulator knob to change the position of the evaporation plate in case more
- than one metal needs to be evaporated (which is our case!);
- Electrode Front-Off-Rear knob to heat the filament of the Front or Rear electrode;
- Power On-Off knob for turning on-off the filament.

Procedure: Wear latex gloves and use metal tweezers to put one piece of Cr on the rear-electrode and 2 cm length of Au on the front-electrode. Load the "loaded plate" at the center-pole of the vacuum chamber on the top of the rear-electrode. Now, close the dome of a vacuum chamber.

To vacuum the evaporation chamber, press the OPERATE button. It will take about 30-40 minutes to completely vacuum the chamber. When you see the needle in the pressure gauge reaching the minimum value, you know that the chamber is ready for evaporation.

Now turn the power knob to ON, the electrode knob to rear, and the current knob to 4-6 (in the 0-9 scale). Allow the Cr to evaporate for 20 secs. Now, use the manipulator to bring the evaporation plate on the top of the Front-electrode (where Au is kept). Bring the current-knob to zero. Move the electrode knob to "Front" and then current knob to 6. Now, look at your watch for 15 secs. The gold evaporates and deposits now. Turn off the Current, Electrode, and Power-knobs.

Press the CHANGE button to get rid of vacuum in the chamber. After 1-2 minutes, you can take out your evaporation plate. Now, close the dome of the evaporator and press the STOP button.

2.5.5. Liquid Cell Cleaning:

Liquid cell cleaning after the end of each experiment is a good practice. Also, if it has not been used for more than several days, then clean it before starting a new experiment. To do that, remove any cantilever chips safely and put them in a box. Pour ethanol on the LC in the center region and tubing. Next, repeat with much more water. The quantity of water used should be about 3-4 times more than the ethanol used. Repeat this procedure several times. Dry the LC using pure N_2 gas. Don't use full pressure in the outlet pipe for this procedure. Keep the regulator position halfway.

Chapter 3: Calibration and testing of our SMFS-AFM

This chapter starts with a brief description of proteins and expression of the I27 protein. It is followed by spring constant calibration of the cantilever. Then the FX and FC calibration experiments using the I27 protein are described. The chapter ends with the calculation of force and deflection sensitivity of our AFM.

3.1 $(I27)_4$ polyprotein as an AFM calibration standard:

$(I27)_4$ is a recombinant polyprotein composed of four repeats of Ig 27 domain of human cardiac titin. A lot of studies have been done on the I27 protein[1-5]. So, it was a natural choice as a reference standard to calibrate our custom built AFM.

Proteins are composed of amino acids linked together via peptide bonds. An amino acid consists of three parts: an amino group NH_2 at one end, a carboxyl group COOH at the other end, and a central carbon atom (α carbon) with an alkyl group R. There are 20 native amino acids differing in R. Proteins are produced by the condensation of monomers (amino acids) to form polymer (protein) where water is a by-product (fig 3.1). Proteins are an important group of biopolymers because they do the majority of functions in living organisms. A protein usually consists of 30-400 amino acids.
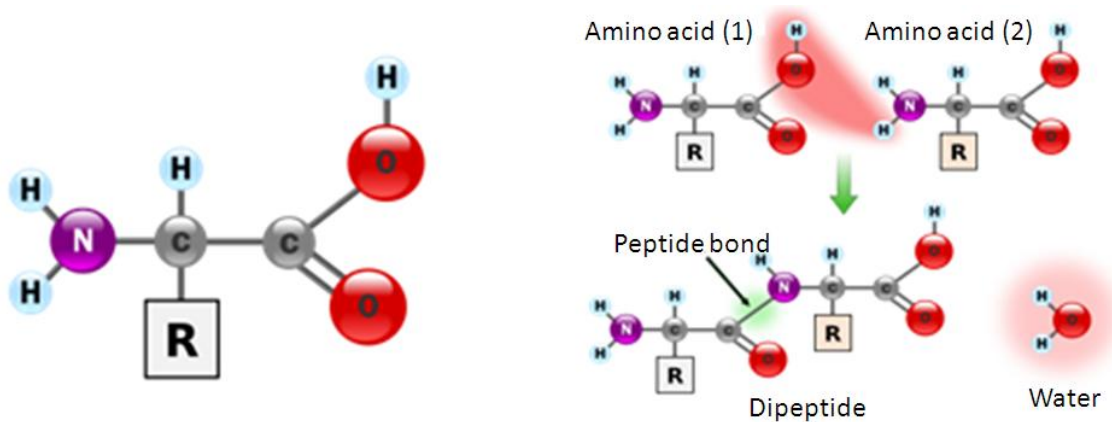
Fig 3.1 Amino acid and the reaction of condensation and formation of peptide bond. Adapted from www.wikipedia.org

Most of the proteins get folded into a particular 3-dimensional structure. That shape is called the native conformation. Four different aspects of a protein's structure are known, namely the primary, secondary, tertiary and quaternary structure. Primary structure is simply the amino acid sequence. Secondary structure is comprised of alpha helices, beta sheets, and turns, stabilized by hydrogen bonds. Elements of secondary structure link with one another to form a functionalized domain of a proteins, which is often called a tertiary structure. More complicated proteins, e.g. hemoglobin, have several domains linked together to form a quaternary structure.

The expression and purification of the $(I27)_4$ protein is described as follows from ref[5]. Multiple rounds of successive cloning were used to create an N-C linked, four-domain polyprotein gene of $(I27)_4$. This gene was encoded in vector pQE30 and expressed in E. coli strain BL21-(DE3). Pelleted cells were lysed by sonication. The His-tagged protein was purified using first an immobilized Talon-Co^{2+} column from Clontech and then by gel filtration on a Superdex 200 column. This purified protein was verified by SDS-PAGE. Finally, it was stored in a PBS buffer at 4°C. This part of the study was performed in collaboration with Dr. Anna

Zolkiewska and Dr. Michal Zolkiewski of the biochemistry department at Kansas State University.
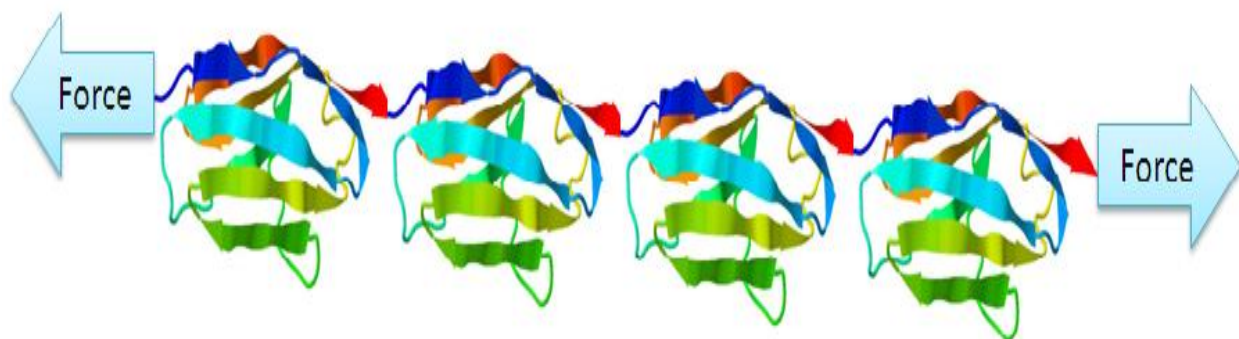
Fig 3.2 The illustration of (I27)$_4$ construct comprising four modules of I27 linked in series. Adapted from protein data bank (PDB) code 1TIT. The direction of the applied stretching force is shown.

3.2 Calibration of spring constant of a cantilever:

The spring constant of the cantilever needs to be known for a precise measurement of force. The manufacturer provides a nominal value of the spring constant of cantilever, which might differ significantly from its actual spring constant. In our set-up, the spring constant was found using the "thermal method" given by Hutter and Bechhoefer[6-7]

$$k = \frac{k_B T}{<x^2>} = \frac{k_B T}{Power * Slope^2}$$ ..(3.1)

where k_B is the Boltzmann's constant,

T is temperature in absolute scale,

$<x^2> = (Power)*(Slope)^2$ is the mean square deflection of the cantilever, where "Power" is the area under the fundamental resonant frequency and "slope" is the ratio of extension (in nm) to force (in volts) when the cantilever is in contact with the surface.

Power spectrum: For a given signal, the power spectrum gives a plot of the portion of a signal's power falling within given frequency bins. The most common way of generating a power spectrum is by using a discrete Fourier transform. The plot is Power (in dB) vs. Frequency (in Hz, but in the log scale). So it is a log-log plot. A power spectrum is obtained following the procedure described in section 2.4.2(J). A typical power spectrum of MLCT type D lever in liquid is shown in fig 2.13. The fundamental resonant frequency and the "Power" are shown in the figure.

Calibration of slope: Slope calibration was obtained following the procedure described in section 2.4.2(L) and fig 2.14.

3.3 The FX calibration experiments:

Several FX experiments on (I27)$_4$ were done to see the performance of our custom built single molecule AFM. (I27)$_4$ in a Phosphate Buffered Saline (PBS) buffer was deposited on a glass cover slip freshly coated with gold. The MLCT type D cantilever was used to obtain calibrated FX traces. The FX experiment was done as described in the section 2.4.2. The calibration

procedure consisted of obtaining the calibrated FX traces of $(I27)_4$. The results of the FX experiment were fitted using the WLC model and compared with literature values. (Fig 3.3)

3.3.1 Calibration of force and extension:
The raw data for both force and extension are obtained in volts, but we want the force and extension in their natural units, Newtons and meters, respectively, or rather in pN and nm as they are the relevant magnitude of force and extension in our experiments.
Force (F) in pN is obtained by

$$F[pN] = F[V] * Slope[\frac{nm}{V}] * k[\frac{pN}{nm}]$$ ..(3.2)

where k stands for the spring constant of the cantilever. And Extension (Ex) in nm is obtained by

$$Ex[nm] = Slope[\frac{nm}{V}] * (Ex[V] - F[V])$$ ..(3.3)

The 2nd term in equation (3.3), i.e. $Slope[\frac{nm}{V}] * F[V]$, is the cantilever displacement which needs to be subtracted to get corrected Extension.
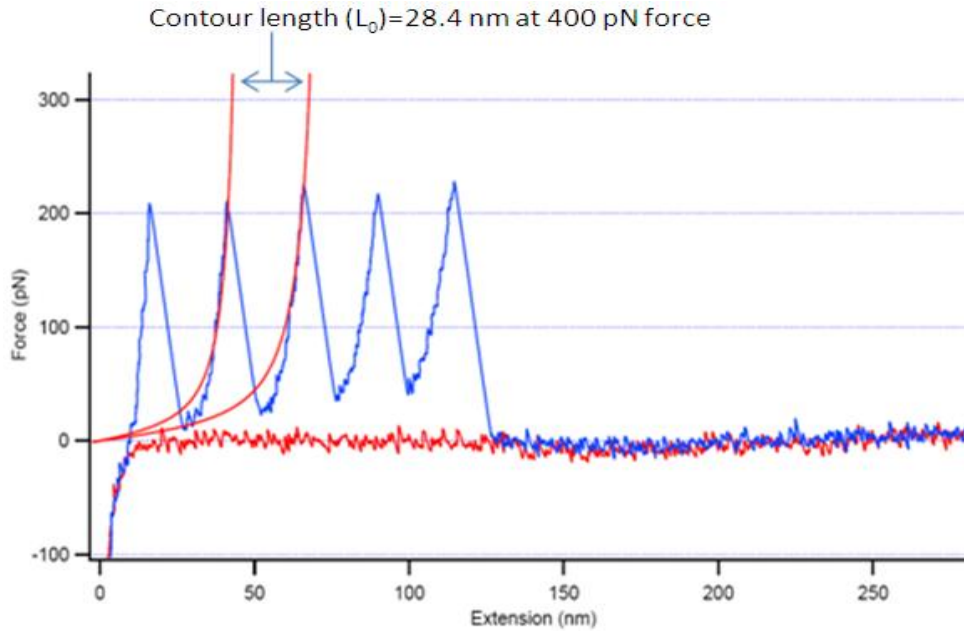
Fig 3.3 A calibrated and corrected FX trace of pulling of $(I27)_4$ polyprotein. This figure consists of saw-tooth like behavior. Every tooth corresponds to the unfolding of one I27 module by force. The last peak shows the contact rupture. Then it was fitted with WLC model. We found the unfolding force ~ 200 pN. The contour length of each I27 is 28.4 +/- 1.5 nm and the persistence length P=0.39 +/- 0.01 nm.

3.3.2 Information obtained from the FX traces of $(I27)_4$:
The values of persistence length (P), unfolding force (F) and contour length (L_o) of a monomer of $(I27)_4$ can be obtained from a calibrated FX trace by fitting the Worm Like Chain (WLC) model of polymer elasticity. The formula that describes the extension x of a WLC with contour length L_o and persistence length P for stretching force F is[8]:

23

$$\frac{FP}{k_BT} = \frac{1}{4}\left(1 - \frac{x}{L_0}\right)^{-2} - \frac{1}{4} + \frac{x}{L_0}$$

..(3.4)

Where: k_B is the Boltzmann's constant and T is the temperature in the absolute scale.

WLC model of polymer elasticity is often used in analyzing the elastic properties of DNAs[8] and polyproteins[9]. Persistence length is the maximum length of the uninterrupted polymer chain persisting in particular direction. The contour length of a polymer is its length at maximum physically possible extension. For I27, persistence length is $0.39+/-0.07$ nm[2].

From literature[2], the unfolding force of I27 is 204 +/- 26 pN and contour length is 28.4+/-1.5 nm. We found the same unfolding force and contour length in our FX calibration experiment by fitting with WLC model. Persistence length was found to be 0.39 +/- 0.01 nm.

3.4 The FC calibration experiments:

In addition to the FX calibration experiment, the FC calibration experiment was also performed. Fig 3.5 shows a FC calibration trace. Length (L) is the end-to-end length of the (I27)$_4$ protein. A force of 190 pN was used in the FC calibration experiment. From literature[10], we expected that unfolding of (I27)$_4$ should yield 23.6 nm steps in L vs. time graph and we got the same. Feedback optimization is important so that the microscope shows the forces which are applied to it. For example, after feedback optimization, we should get 100 pN when we apply 100 pN in pulling. More advanced calibration in FC mode would consist of getting several FC traces at every given point of force and calculating the I27 unfolding rate constants, which are also tabulated in literature.
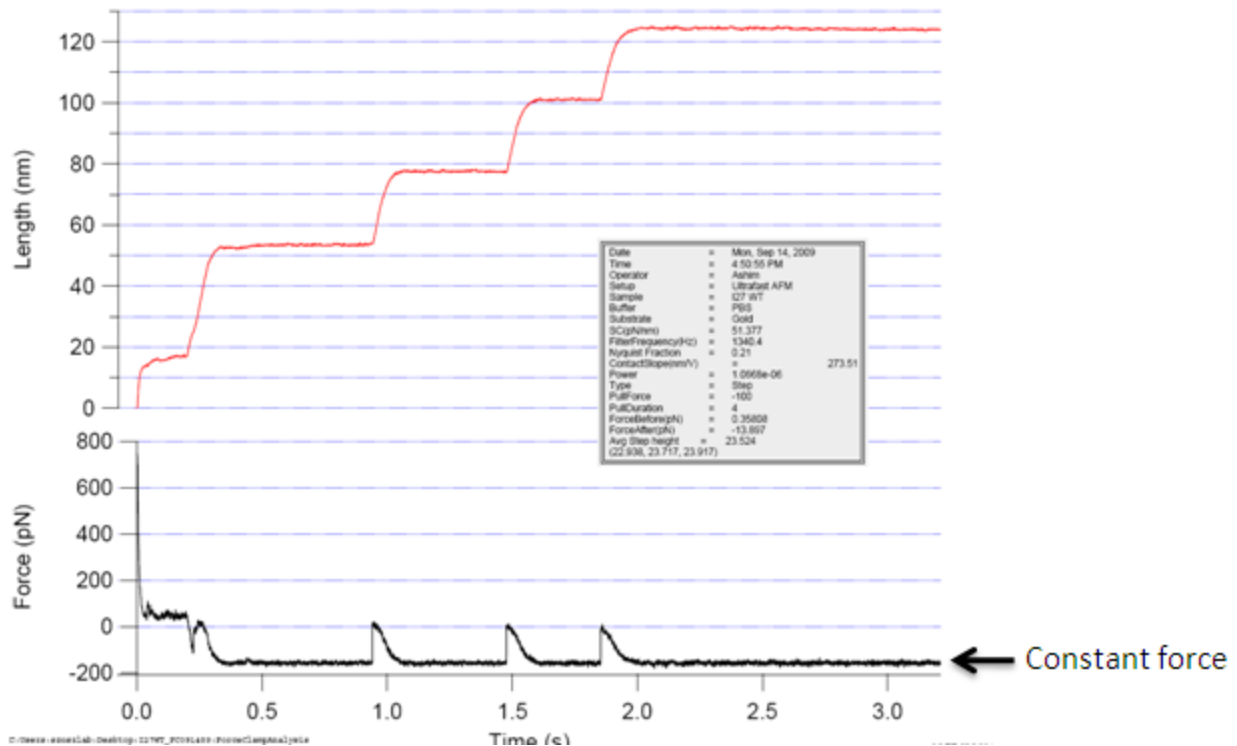
Fig 3.4 A FC calibration trace showing Length(nm) vs. Time(s) and Force(pN) vs. Time(s) graphs.

24

3.5 Calculation of force sensitivity and displacement sensitivity of the AFM:

The thermal noise deflection sensitivity as measured by the amount of the thermal noise is given by[11]:

$$\Delta x_{rms} = \sqrt{\frac{4\beta k_B T(BW)}{k^2}} = \sqrt{\frac{2k_B T(BW)}{\pi f_o Qk}} \qquad ..(3.5)$$

where,

k = Spring constant of the cantilever = 50pN/nm for MLCT type D,

k_B = Boltzmann's constant,

T = Experimental temperature in absolute scale = 300K,

BW = Bandwidth of the experiment = 350 Hz and

β = Drag coefficient = $\dfrac{k}{2\pi f_o Q}$

f_0 = Fundamental resonant frequency of free vibration of the cantilever = 3 kHz for MLCT type-D,

Q= Mechanical quality factor of free vibration of the cantilever = 1.71 (calculated from a typical power spectrum of MLCT type D)

and force sensitivity is given by:

$$\Delta F_{rms} = \sqrt{\frac{2kk_B T(BW)}{\pi f_o Qk}} \qquad ..(3.6)$$

Using the above values in equation (3.5) and (3.6), we calculated the force sensitivity to be 3 pN and deflection sensitivity to be 60 pm. These values correspond to the thermal noise only. The force sensitivity and deflection sensitivity we calculated from the experimental FX trace was ~12 pN and 240 pm, respectively, at the BW of 350 Hz. These values correspond to the overall noise of the system including mechanical and electronic noise, in addition to the thermal noise.

References:

1. M. Rief, M. Gautel, F. Oesterhelt, J. M. Fernandez, H. E. Gaub, Reversible unfolding of individual immunoglobin domains by AFM. Science 276, 1109–1112 (1997).

2. M. Carrion-Vazquez, A.F. Oberhauser, S.B. Fowler, P.E. Marszalek, S.E. Broedel, Jr. J. Clarke, and J.M. Fernandez. Mechanical and chemical unfolding of a single protein: a comparison. PNAS USA. 96(7):3694-3699 (1999)

3. T.E. Fisher, P.E. Marszalek and J.M. Fernandez, Stretching single molecules into novel conformations using the atomic force microscope. Nature Struct. Biol. 7, 719–724 (2000).

4. H. Li, W.A. Linke, A.F. Oberhauser, M. Carrion-Vazquez, J. G. Kerkvliet, H. Lu, P.E. Marszalek and J.M. Fernandez, Reverse engineering of the giant muscle protein titin, Nature, 418, 998-1002 (2002)

5. R. Szoszkiewicz. S.R.K. Ainavarapu, A.P. Wiita, R. Perez-Jimenez, J.M. Sanchez-Ruiz and J.M. Fernandez, Dwell Time Analysis of a Single-Molecule Mechanochemical Reaction, Langmuir, 24, 1356-1364 (2008)

6. L. Hutter, J. Bechhoefer, Calibration of atomic force microscope tips, Rev. Sci. Inst., 64, 1863-1873, (1993).

7. R. Levy, M. Maaloum, Measuring the spring constant of atomic force microscope cantilevers: thermal fluctuations and other methods, Nanotechnology,13, 33-37, (2002).

8. C. Bustamante, J. Marko, E. Siggia, S. Smith, Science, 265, 1599-1600, (1994)

9. L.Tskhovrebova, J. Trinick, J.A.Sleep and R.M. Simmons. Elasticity and unfolding of singlemolecules of the giant muscle protein titin. Nature 387, 308±312 (1997).

10. A.P. Wiita, S.R.K. Ainavarapu, H.H. Huang and J.M. Fernandez. Force-dependent chemical kinetics of disulfide bond reduction observed with single-molecule techniques, PNAS USA. 103(19):7222-7227 (2006).

11. W. J. Greenleaf, M.T. Woodside and S.M. Block. High-resolution, single-molecule measurements of biomolecular motion. Annu. Rev. Bioph. Biom. 36, 171-190 (2007).

Chapter 4: FX Study of Notch protein

4.1. Background and motivation for Notch studies:

Notch is a transmembrane protein. The negative regulatory region (NRR) of Notch has 221 to 289 amino acids. Notch is responsible for cell signaling processes. Notch signaling in aberrant way has few oncogenic roles in breast cancer[1,2]. Aberrant signaling means that there will not be any cuts at S2 and S3 sites (see fig 4.1). Notch signaling triggers self-renewal of stem-like cells during the pre-invasive stage of the disease[2]. Notch signaling moderates hypoxia-induced tumor cell migration and invasion. Finally, Notch plays a pro-angiogenic role in tumor endothelial cells. Overall, the Notch signaling pathway is a prominent therapeutic target in breast cancer[3].
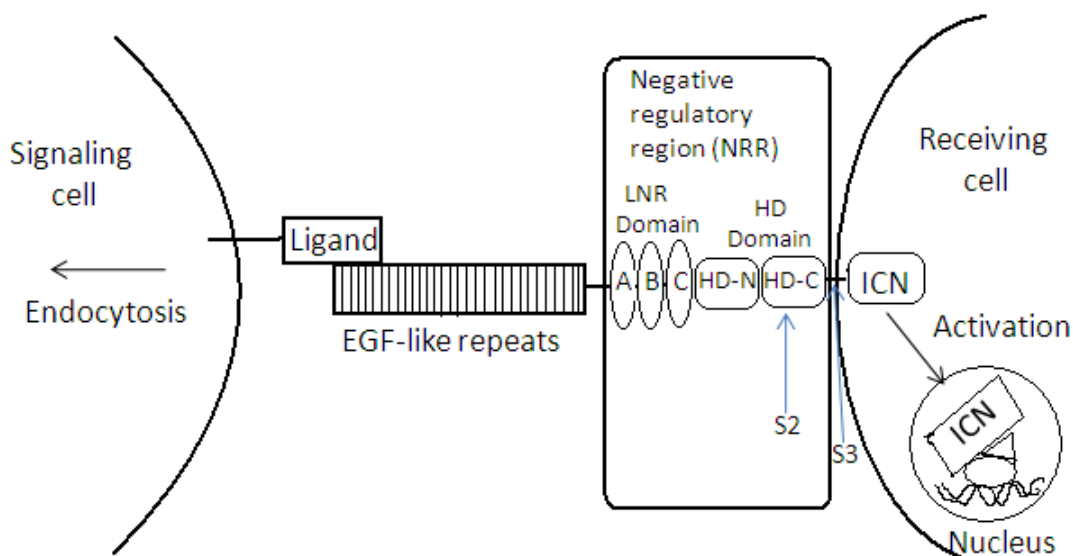
Fig.4.1 Overview of Notch signaling. The portion of Notch we studied was the Negative Regulatory Region (NRR) showed in the figure. It is proposed that ligand endocytosis exerts a pulling force on a Notch receptor and triggers its cleavage at the S2 site by an ADAM protease. In our FX experiment, studies on Notch activation was done by mimicking the ligand pulling by AFM cantilever pulling.

Activation of Notch pathway occurs when the ligand at the surface of a signal-sending cell binds to a Notch receptor in a signal-receiving cell (see fig 4.1). This is followed by a sequential cleavage of Notch receptor at the S2 site in the extracellular domain by an ADAM (A Distintegrin And Metalloprotease) protease and subsequently at S3 site in the transmembrane domain by γ-secretase[4,5]. Both the S2 and S3 sites pertain to the peptide bonds in a series of well specified amino acids. Cleavage by γ- secretase triggers the displacement of the intracellular domain of Notch (ICN) to the nucleus. Once ICN gets inside the nucleus, it activates target gene expression.

An essential step in Notch activation is a cleavage at the S2 site which requires ligand binding[6]. It has been postulated that the ligand needs to undergo endocytosis in the signal-sending cell in order to activate the Notch receptor[7,8]. Recent data from X-ray crystallography on human Notch showed that a ligand-free Notch is protease-resistant in a conserved NRR.

To the best of our knowledge, no earlier attempts at Notch activation by applying a mechanical force on the NRR region via single molecule AFM have been performed. From our

AFM experiments, we expect to get the information about the Notch signaling pathway. We want to make sure to verify if mechanical force exposes S2 site. However, our AFM experiments would not lead to treatments, prevention or better drugs for breast cancer patients at this initial point of study. The family of Notch proteins comprises four members. We have investigated an NRR from Notch 1.

4.2. Construct of the $I27_2 - NRR - I27_2$

We have synthesized the DNA construct encoding $I27_2 - NRR - I27_2$, where the human NRR1 domain of Notch is flanked by the sequence of I27 (see section 3.1) repeated twice on both ends of NRR region. The I27 handles provide controlled force delivery to the NRR termini (fig 4.2).

The following procedure was followed to express $I27_2 - NRR - I27_2$. The corresponding cDNA fragments were amplified by PCR using human cDNA and PfuTurbo DNA polymerase, and subcloned into the pET15b vector containing a 6xHis tag. The recombinant proteins were expressed in Rosetta(DE3)pLysS *E. coli* and affinity-purified on nickel columns. If inclusion bodies were formed, proteins were recovered from the insoluble fractions as described in the Ref. 10. The proper folding of the purified proteins was verified by using circular dichroism and differential scanning calorimetry. This part of the study was performed in collaboration with Dr. Anna Zolkiewska and Dr. Michal Zolkiewski of the Kansas State University Biochemistry department.
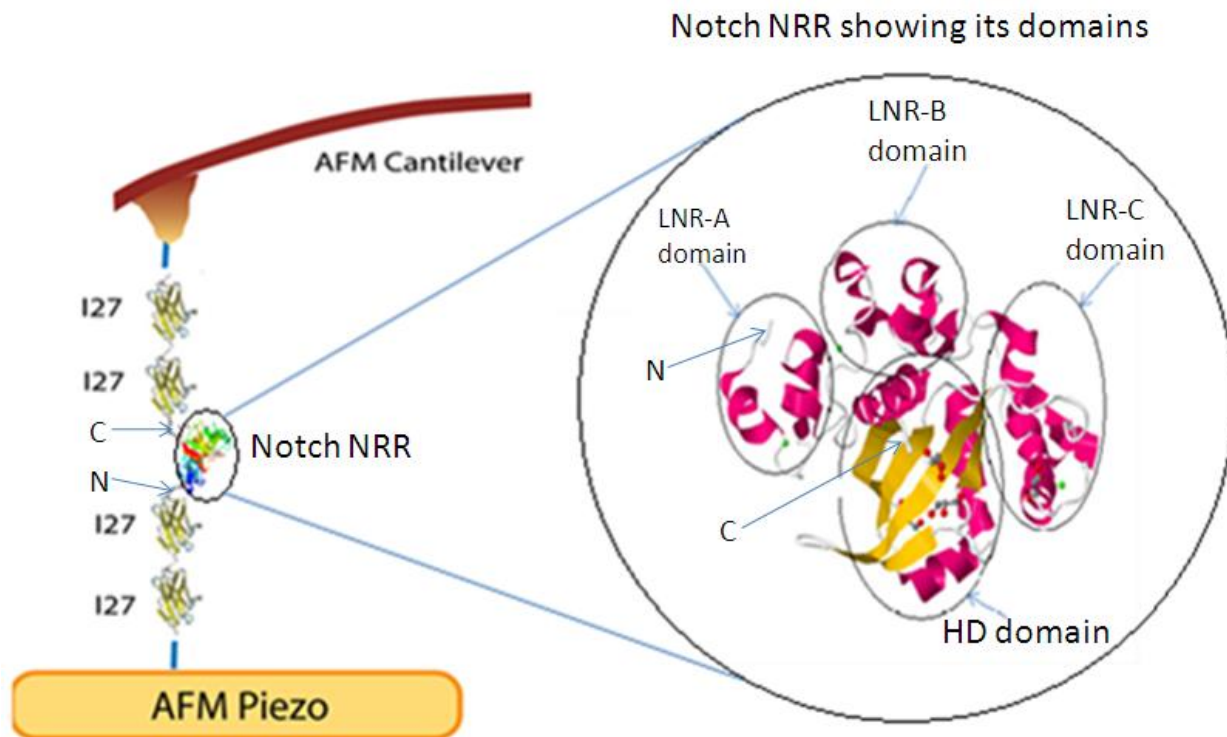
Fig.4.2 (A) Schematic diagram of pulling of the $I27_2 - NRR - I27_2$ protein construct by single molecule AFM. (B) The illustration of Human Notch 1 showing secondary structure from Protein Data Bank (pdb code 3ETO). This image was processed using Jmol software. The ash colored spheres represent carbon atoms while the red spheres represent oxygen atoms and green spheres represent calcium. Pink spirals represent α-helices and yellow strips represent β-strands. Notch 1 is divided into LNR-A, LNR-B, LNR-C and HD domains. HD domain is further divided into HD-N and HD-C domains (see fig 4.1)

4.3. FX experiment on the Notch construct:

The Notch construct was investigated in the FX mode with a pulling speed of 400 nm/s (see section 2.4.2 for details of FX experiments). Gold evaporated glass cover-slips were used as substrates (see section 2.5.4). For each experiment ~ 30 µl of Notch construct in a PBS buffer was deposited on the substrate. We used MLCT-D cantilevers from Veeco with an elastic spring constant of 50 pN/nm.

In our FX experiments, $I27_2 - NRR - I27_2$ was clamped between an AFM tip and a gold substrate by random pick-up. As the AFM tip withdraws from the substrate surface, mechanically induced conformation transitions of a Notch construct are measured by recording the force and instantaneous extension of an AFM cantilever.

Fig 4.4 shows two representative traces. We recorded 60 acceptable FX traces in total. The acceptable traces are characterized by low interference (small oscillations in force), low noise, lack of initial surface adhesion peaks, and at least two I27 unfolding peaks.
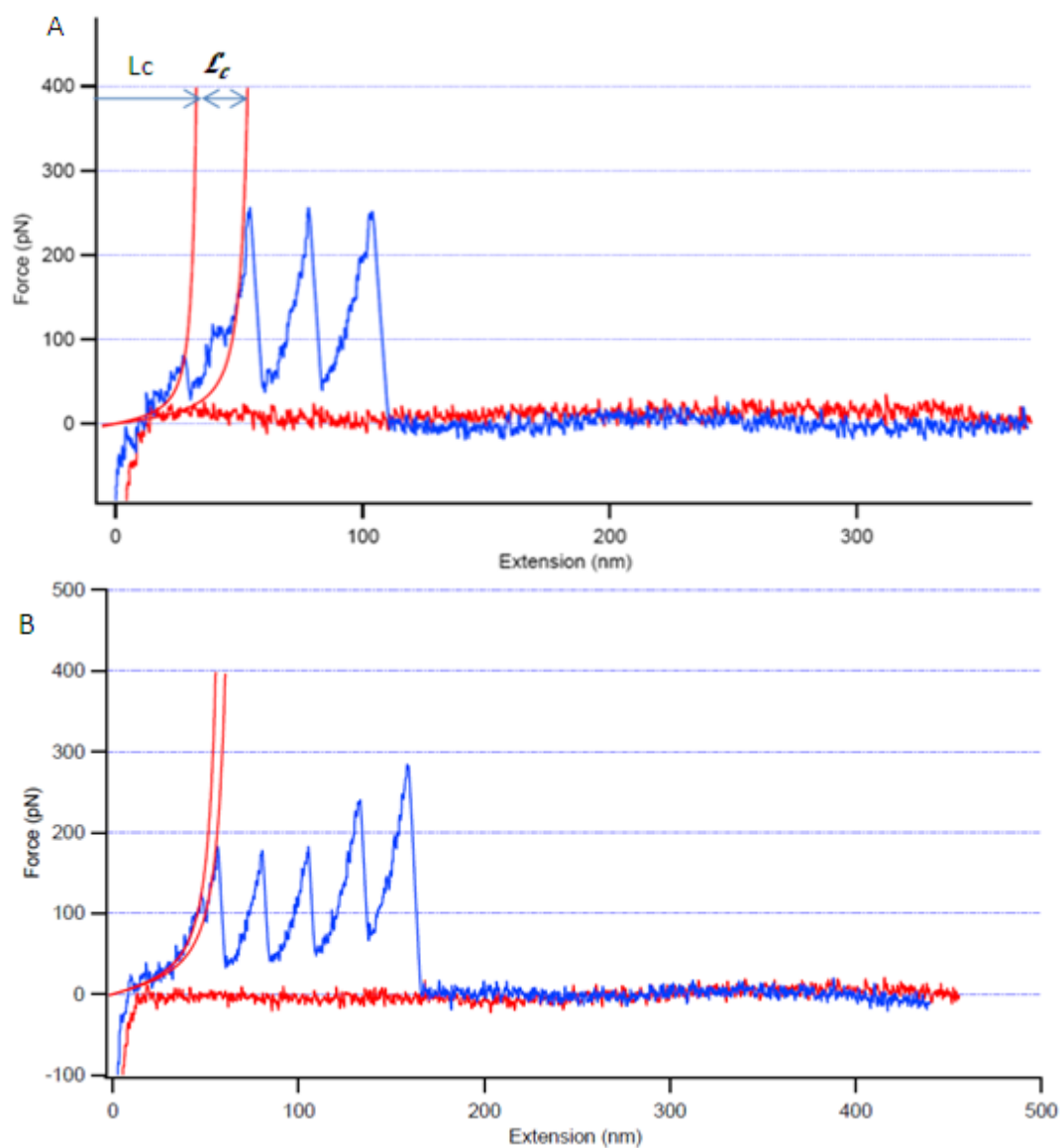
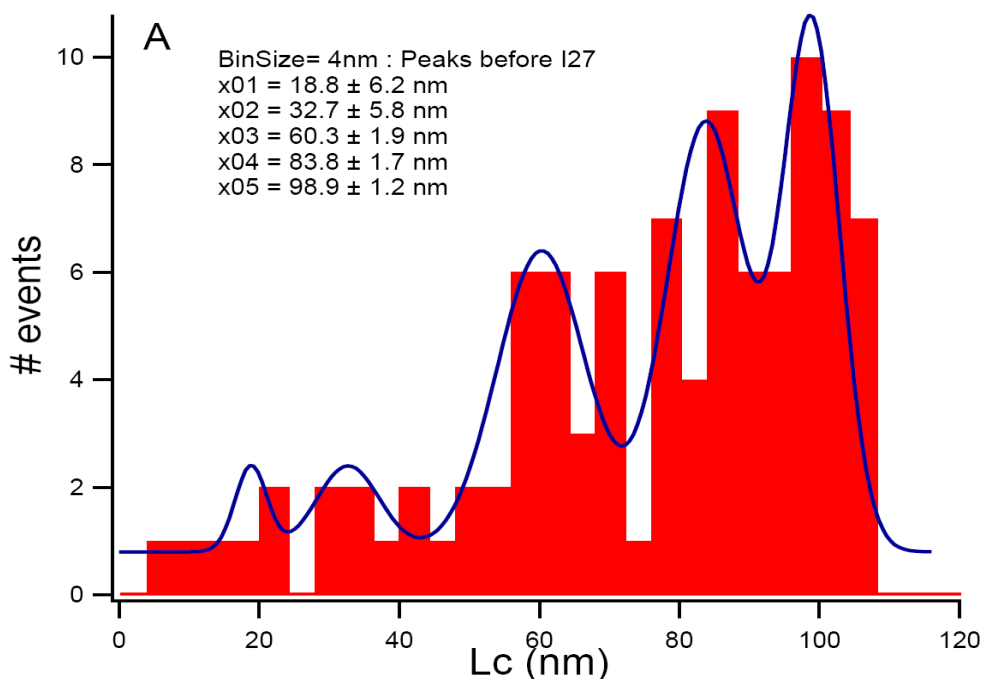**Fig.4.3** Representative traces of the Notch FX experiment.
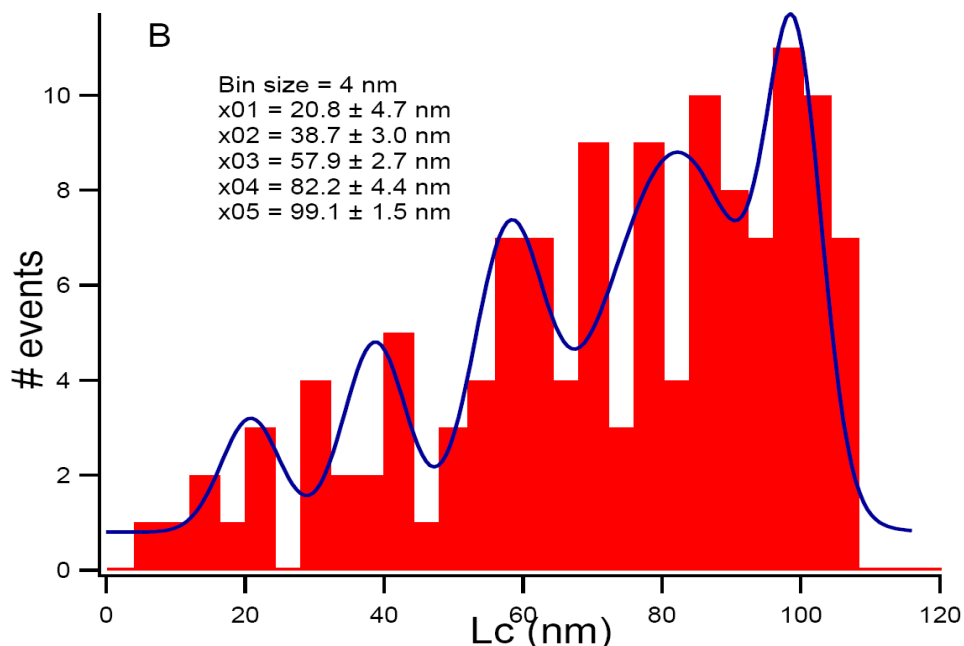
4.4. Analysis of the experimental traces:

4.4.1. Extension Analysis:

The FX traces were calibrated and corrected so that the extension variable plots only the end-to-end length of the Notch construct. Other force peaks (not coming from I27) were attributed to conformational transitions of the Notch protein itself. For the Notch peak(s) occurring before the first I27 peak, the contour length increment $\mathcal{L}_c$ was measured as the distance between the Notch peak to the first I27 peak. For any Notch peak(s) occurring in between the I27 peaks, the $\mathcal{L}_c$ was measured from the nearest I27 peak.

     A program was written so that the values of $\mathcal{L}_c$ were found at the force of 400 pN (see fig 4.3(A)) by fitting the WLC model to the respective force peaks. At 400 pN, however, any WLC fitted portion of a protein is unfolded at 95% of its contour length (see eqn 3.4), so we calculated the $\mathcal{L}_c$ corresponding to 100% unfolding or entire stretching of the portion of the protein in question.

     Next, we wanted to plot the increase in the N-C distance, Lc, of the unfolding Notch protein. To do that, the value of $\mathcal{L}_c$ was subtracted from the total stretched length of Notch obtained by multiplying the number of amino acid residues by 0.4 nm. For example, our Notch has 289 amino acids, so its total stretched length is 289*0.4 = 115.6 nm, and Lc = (115.6 - $\mathcal{L}_c$) nm. We fitted 5 Gaussian peaks because we expected one peak corresponding to each of the LNR domains A, B and C and two peaks for HD domain.

A

BinSize= 4nm : Peaks before I27
x01 = 18.8 ± 6.2 nm
x02 = 32.7 ± 5.8 nm
x03 = 60.3 ± 1.9 nm
x04 = 83.8 ± 1.7 nm
x05 = 98.9 ± 1.2 nm

Fig.4.4 Histograms of the contour length increments observed in Notch by taking the "resting length" of Notch as zero contour length. (A) shows the data corresponding to Notch attributed peaks before I27 peaks only and (B) shows the data corresponding to all Notch attributed peaks.

4.4.2. Force measurements:

Force histograms for bin size of 5 pN and 10 pN were plotted (fig 4.5). A curve having six Gaussian traces was fitted with a confidence level of 95%. The force peaks for Notch were found at 22.4 ± 4.9 pN, 40.0 ± 3.7 pN, 56.9 ± 3.6 pN, 98.5 ± 2.2 pN, 162.3 ± 2.3 pN and 213.3 ± 1.2 pN. This shows that mechanically stable conformational transition states of different Notch domains requires different forces varying from 22.4 ± 4.9 pN to 213.3 ± 1.2 pN.
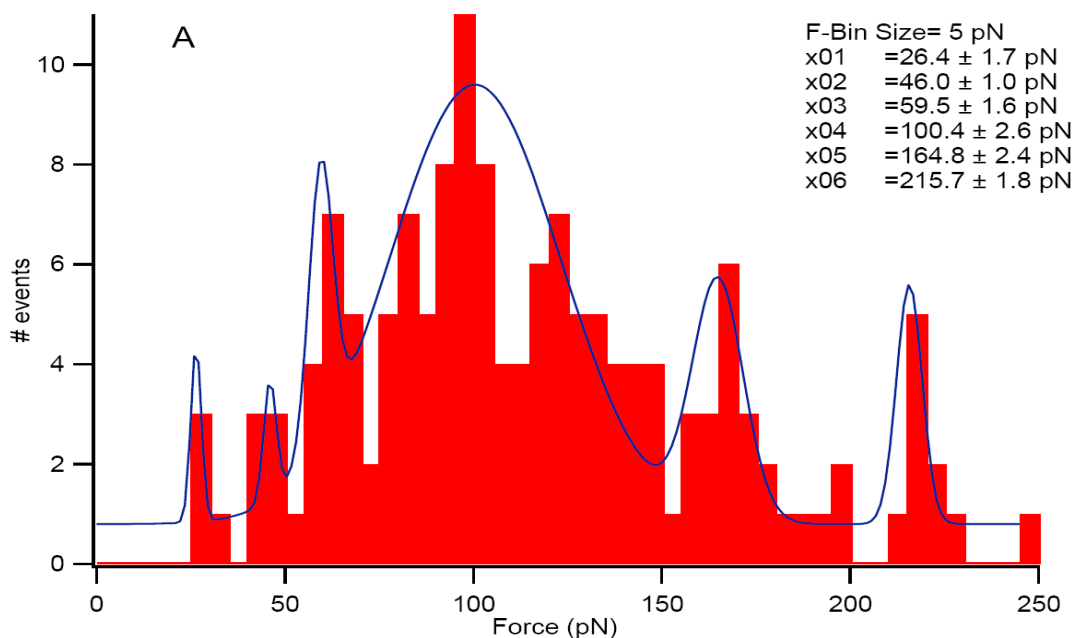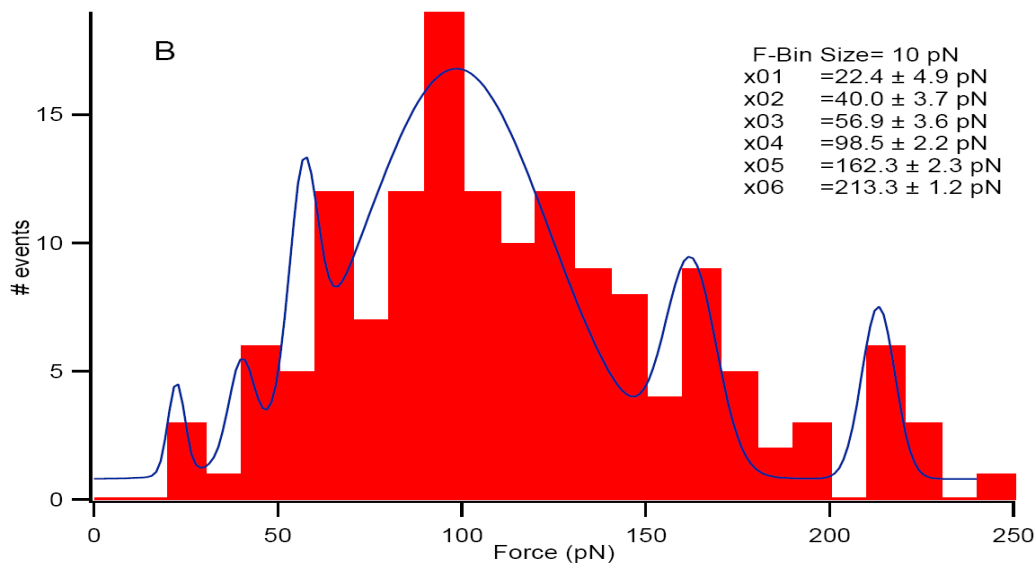
Fig.4.5. Distribution of the unfolding force peaks attributed to Notch.

In order to interpret our data, we compared this data with molecular dynamics simulations (see section 4.5). We also calculated the values of Lc based on the X-ray structural data of the NRR region (see section 4.6).

4.5. Numerical simulation:

We collaborated with Dr. Jianhan Chen from Biochemistry department at KSU for numerical simulation of this experiment. The following plots are the outcomes of his steered molecular dynamics simulation. Fig. 4.6 is a simulation plot of average force as a function of N-C distance in Notch, computed at three different pulling speeds.
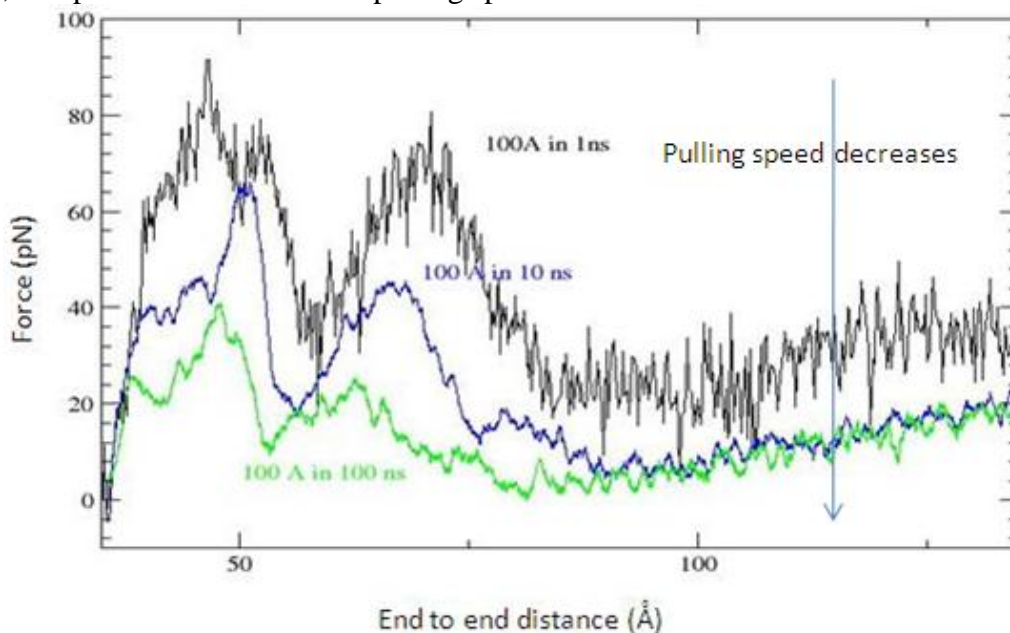
Fig. 4.6 Numerical simulation plot of average force as a function of N-C distance of Notch, computed at three different pulling speeds.

Several force peaks can be identified in fig 4.5. The x-axis of this graph starts at 35Å which is the 3ETO.pdb native N-C distance.

Black line: Pulling speed is 10^{10} nm/s, which is 8 orders of magnitude higher than our AFM pulling speed. Peaks are found at 47Å, 53Å and 71Å

Blue line: Pulling speed is 10^{9} nm/s, which is 7 orders of magnitude higher than our AFM pulling speed. Peaks are found at 50Å, 68Å and 79Å.

Green line: Pulling speed is 10^{8} nm/s, which is 6 orders of magnitude higher than our AFM pulling speed. Peaks are found at 38Å, 48Å and 63Å.

Fig 4.7 is a simulation plot of average force as a function of the N-C distance for Notch, computed from 31 pulling simulations. The pulling speed is 10^{5} nm/s, which is only 3 orders of magnitudes higher than our AFM pulling speeds. Each pulling took about 50 hours to simulate. The black lines shows the force from overall simulation and the red line shows the average force.
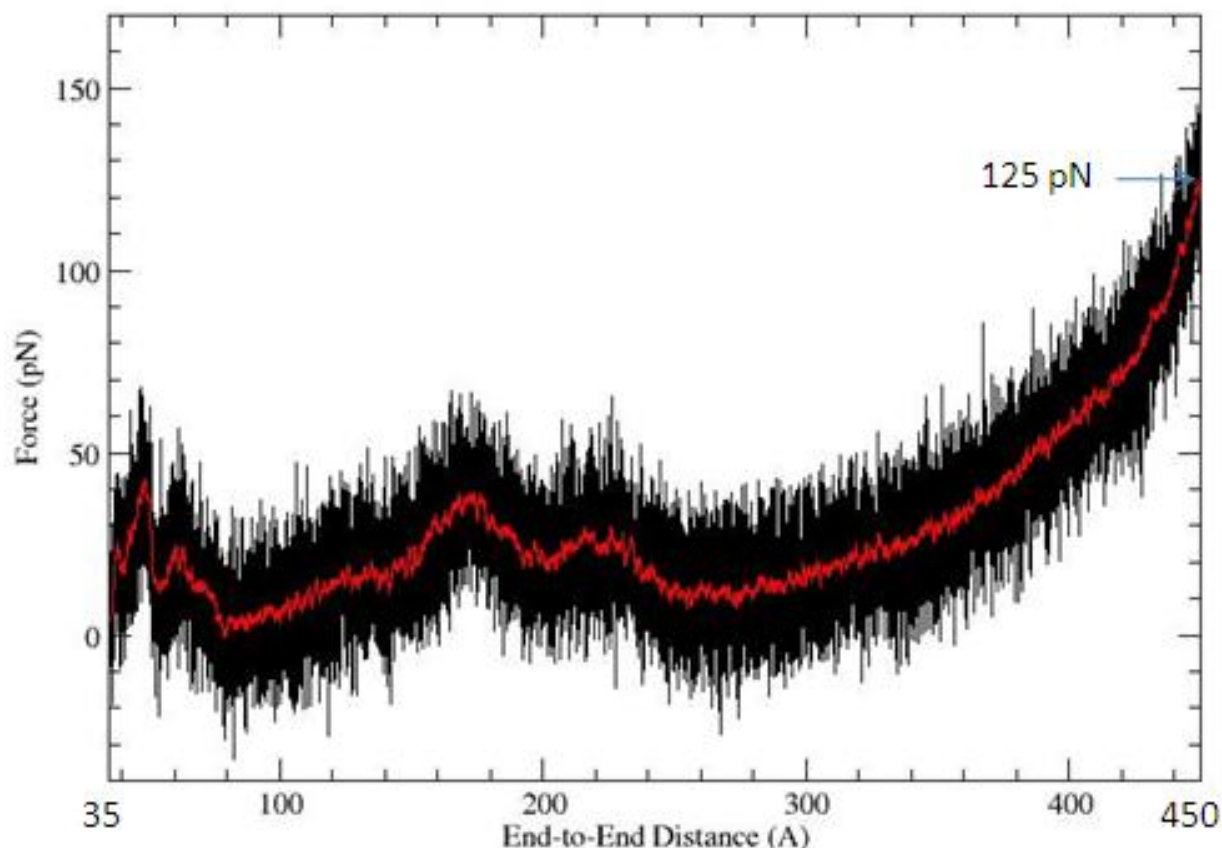
Fig.4.7. Numerical simulation plot of average force as a function of N-C distance of Notch computed at pulling speed of 10^{5} nm/s (10^{-4} m/s).

Several "landmarks" can be identified in this graph as presented in Figs.4.7 and 4.8. The errors are estimated be 0.5 nm, which is roughly the size of one residue:

a) 3.5 ± 0.5 nm: 3ETO.pdb native N-C distance (Note that the End-to-End distance axis of the plot starts from 35 Å)

b) 4.5 ± 0.5 nm: just before the LNR-A detachment

c) 6.5 ± 0.5 nm: just before the LNR-B detachment

d) 13.0 ± 0.5 nm: just before the LNR-C detachment (no peak observed; it also appears the easiest to detach the third domain, see Fig. 4.7)

e) 17.0 ± 0.5 nm: just before the C-terminal beta-strand pops-out (this concerns some unfolding from within HD domain)

f) 22.0 ± 1 nm: just before C-terminal alpha-helix pops-out from HD domain (mild peaks ~ 21 & 23 nm)

g) ~50 nm: "maximal" length before breaking disulfide bonds between all the cysteines.
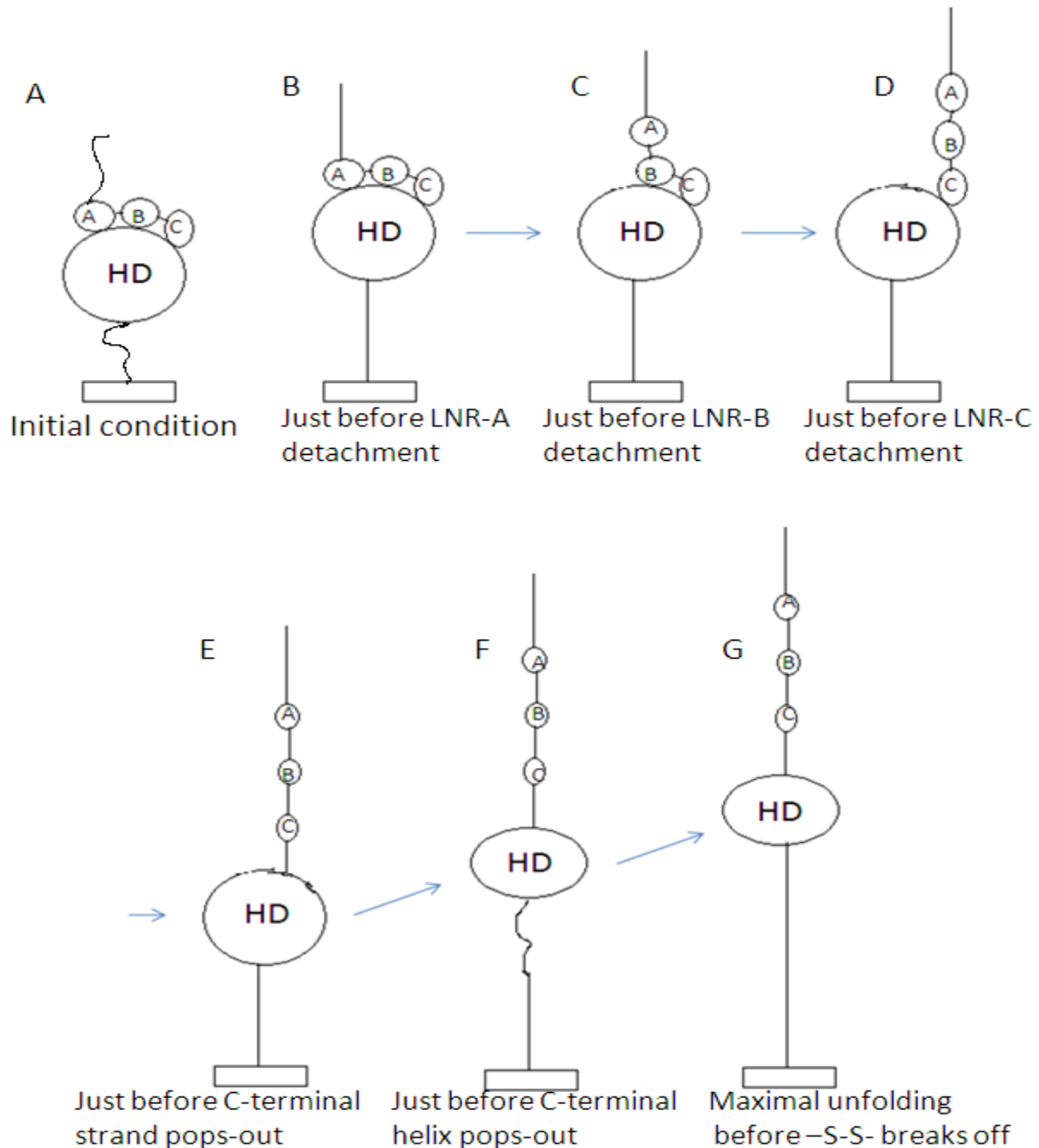
Fig 4.8 Visualization of the landmarks in the molecular dynamics simulation study. Fully unfolded NRR length without disulfide bonds rupture (drawing G) is expected to be 50 nm. With all the disulfide bonds ruptured the contour length of 115 nm is expected.

34

4.6. Theoretical Calculations of Lc based on number of amino acid residues:

In this section we estimate the values of Lc obtained when certain regions of Notch unfold and fully stretch. For visual understanding of the analysis, presented below, please consult Fig.4.2(B) and Fig. 4.8.

Our initial assumptions are as follows. First, the length of each amino acid is taken to be 0.4 nm. Second, we expect a peak force to mark a NRR conformation which is just about to undergo a partial unfolding event. Third, each LNR domain has three disulfide bonds, which are covalent. Based on the literature[11], these disulfide bonds should not break below 1-1.5 nN of a stretching force. In this way each LNR domain is expected to rather detach from the NRR construct during pulling than to unfold. Same applies to HD domains (also containing some disulfide bonds). Finally, we note that a presented here NRR structure (Figure 4.2(B), pdb code: 3ETO) does not display a loop region comprising 47 amino acids (residues 1623 and 1669). This loop region also contains another particular cleavage site, called the S1 site.

The table below lists the amino acids belonging to each particular domain of Notch. There are 279 residues in the NRR structure itself. They range from 1449 - 1727 (missing part of this pdb containing the S1 site is between residues 1623-1669).

Original sequence id in PDB files 3ETO	Residue in model
LNR-A: 1449-1480	(1-32)
SS bonds: 1450-1473, 1455-1468, 1464-1480)	(2-25, 7-20, 16-32)
Ca: Asp1458, Asp1476, Asp1479	(10, 28, 31)
LNR-B: 1491-1522	(43-74)
SS bonds: 1491-1515, 1497-1510, 1506-1522	(43-67, 49-62, 58-74)
Ca: Asp1503, Asp1507, Asp1518, Asp1521	(55, 59, 70, 73)
LNR-C: 1529-1562	(81-114)
SS bonds: 1529-1555, 1537-1550, 1546-1562	(81-107, 89-102, 98-114)
Ca: Asp1543, Asp1547, Asp1558, Asp1561	(95, 99, 110, 113)
HD: 1568-1727	(120-232)
SS bond: 1686-1693	(191-198)
S2 site: 1722	(227)

The estimates of Lc are as follows:

- **Initial N terminal to C terminal distance**: 3.5 ± 0.5 nm.
- **Just before LNR-A detachment:** This comprises stretching and relocation of two terminal residues. We estimate that the associated Lc change is from 0 to 1 nm, e.g., 0.5 ± 0.5 nm. Comprised here is also elastic stretching of the NRR domain itself. The estimated elasticity constants for simple proteins are typically of the order of 1000 pN/nm[12,13] and the MD force peak associated with this event (Fig. 4.6) is about 40 pN. Based on Hook's law we obtain less than 0.1 nm of elastic extension of the NRR domain, which is negligible. Overall, the expected Lc at which detachment of LNR-A occurs is 3.5+0.5 nm = **4.0 ± 1.0 nm**.
- **Just before LNR-B detachment**: The residues of the LNR-A are stretched and the linkers between LNR-A and LNR-B are stretched. Distance between the residues 1450-1480 which are "trapped" in between the -S-S- bonds is 1.7 ± 0.3 nm (as measured in a VMD software for visualizing pdb files). The distance gained by

detachment of the folded residues 1480 to 1490 is estimated 1.5 ± 0.5 nm (from the PDB file). Thus, the expected Lc at which detachment of LNR-B occurs is $4.0+1.7+1.5$ nm = **7.2 ± 1.8 nm**.

- **Just before LNR-C detachment**: Distance between the residues 1491-1522 which are "trapped" in between the -S-S- bonds is 1.9 ± 0.3 nm. The distance between the folded residues 1523 and 1528 is 1.0 ± 0.5 nm. Thus, the expected Lc just before detachment of LNR-C is $7.2+1.9+1.0$ nm = **10.1 ± 2.6 nm**.
- **Just before popping out of the C-terminal beta-strand**: Distance between the residues 1529-1562 ("trapped" in between the -S-S- bonds in LNR-C) is 1.9 ± 0.3 nm. Length of residues 1563-1568 (linkers between LNR-C and HD) is 1.0 ± 0.5 nm. So, expected Lc of popping out of C-terminal beta strand is $10.1+1.9+1.0$ nm = **13.0 ± 4.4 nm**.
- **Just before popping out of the C-terminal alpha-helix**: We do not have the pdb structure with a beta-strand unfolded, so this distance can be only estimated and expected to **add several nanometers** to the overall N-C distance.

4.7. Discussion and conclusion based on the AFM experiment and simulation:

4.7.1. Force measurements:

Since the outcome of the simulation changes with different pulling speed (see fig. 4.6), only approximate agreement is expected between the FX experiments and the MD simulations. In the FX experimental data, force peaks vary from 20 pN to 220 pN as seen in the force histograms (fig. 4.5). Predominant peak is found at ~100 pN there. In the molecular dynamics simulation study, peaks range from 20 pN to 125 pN (fig 4.7). However, even the slowest presented MD simulation unfolds the protein 1000 times faster than in the FX experiments, so can we do any relevant comparisons?

From fig 4.6, it is evident that the peak force decreases with the decrease in pulling speed. The magnitude of force in a 2nd force peak in the black, blue, green and red traces was 72 pN, 44 pN, 24 pN and 23 pN, respectively. Thus, we can expect even lower force peaks in the FX experiment. The lowest force peak observed experimentally is at ~22 pN and it has only few occurrences. In the light of the displacement measurements (see the next paragraph) it might suggest that we are not able to detect the LNR-A, B, C detachment events.

Quantitative comparison between simulation and experimental data could not be made with current data. For the thermally activated unfolding events a logarithmic dependence of the peak force with a pulling speed is expected. Our data depart from it, as could be quickly seen comparing the evolution of any peak force in the Fig. 4.6. Another reason for a mismatch between simulation data and experimental data is that we are not entirely sure that the detected force peaks come entirely from unfolding of the NRR domain. Other effects, like the non-specific adhesive interactions between the different parts of the protein construct and between the protein and the substrate are possible, as it will be expanded in the next section.

4.7.2. Lc measurements:

The WLC fits on FX traces (fig 4.3) are arbitrary associated with an error of ± 1 nm. In addition, the spring constant and slope calibration has ~5% error. For example, for a contour length of 20 nm, the estimated error would be 2 nm. For larger contour lengths, the error becomes larger.

The predominant values of Lc from the experimental data analysis are 21 nm, 38 nm, 58 nm, 82 nm and 99 nm (see Fig.4.4, 2nd histogram). The predominant Lc values from the

simulation data are 4.5 nm, 6.5 nm, 13 nm, 17 nm, 22 nm, and 50 nm. The only matching values, i.e., 21 nm vs. 17 nm or 22 nm, correspond to peaks marking the partial unfolding from C terminal, i.e., within the HD domain, proceeded by a quick detachment of LNR domains. This is potentially very interesting, since the S2 site (cleaved by ADAMs) is within this region. That implies that mechanical force might indeed be necessary to expose the S2 site for cleavage. We don't see the initial peaks corresponding to the LNR domains detachment. We speculate these events occur at forces below our detection limits. In fact, if we use the picture provided by MD simulations and forget about the unfolding of LNR-A, B and C domains, then popping out of C-terminal helix could be the first detectable peak. From the theoretical calculation (section 4.6), expected Lc for the C-terminal popping out will be at 13 ± 4.4 nm. This is not very far from the molecular dynamics study peak of 17 ± 0.5 nm which also corresponds to the same phenomenon.

In terms of the observed end-to-end extensions, the maximum extension in simulation is 50 nm but it could go till 115 nm if it could unfold entirely. But the contact is breaking before undergoing maximum unfolding. It is unclear why we are getting the extension peaks at higher extension in the experimental data. Possibly, this is another evidence that they are not coming from Notch but from other interactions. The contour length could be taken at the unfolding force instead of using the unfolding force at 400 pN. Another point could be that MD simulation takes the contour length as they are (less than 100% of stretching). But in our experimental data analysis, we use the 100% of the contour length. Besides, there are 279 residues in the NRR structure itself. They range from 1449 - 1727 (missing part of this pdb containing the S1 site is between residues 1623-1669). However, comprising the I27 linkers we have 289 residues in the NRR portion of the construct. Stretching/unfolding of these residues can increase the observed end-to-end lengths by up to 4 nm. Finally, there is no previous FX experiment done on Notch, so we cannot compare it to any existing literature.

4.8. Future work:

The current temporal resolution of the AFM setup, e.g., about 1 ms, is mainly limited by the resonant frequency of a cantilever (~ 1 kHz). To detect a faster process, we need to have a cantilever with higher resonance frequency. Furthermore, unfolding of very small units of proteins might not be seen currently seen in our set-up, which has about 10 pN force sensitivity. These are the future challenges for improved AFM measurements.

The measured here force and distance peaks should be understood in more detail. There are unanswered question like whether the peaks are coming from non-specific surface adhesion between the construct and the surface. For that either specific attachment strategies (e.g. using NHS-PEG-Esters) for the constructs to the surface or different surface should be used. For various surfaces, we will use silicon surface and atomically flat surfaces like Highly Ordered Pyrolytic Graphite (HOPG) and Mica. Also the influence ADAM proteases should be studied by introducing it in the buffer solution. The FC experiments should be done to find the kinetics of S2 cleavage. Then, FC experiment should also be done with ADAMs. We expect a step height and then a cleavage by ADAM. Also, the experiments with different concentration of ADAMs should be performed.

References:

1. W. Shi and A.L. Harris, Notch signaling in breast cancer and tumor angiogenesis: cross-talk and therapeutic potentials. J. Mammary Gland Biol. Neoplasia 11, 41-52. (2006)

2. K. Politi, N. Feirt and J. Kitajewski, Notch in mammary gland development and breast cancer. Semin. Cancer Biol. 14, 341-347. (2004)

3. L. Miele, Rational targeting of Notch signaling in breast cancer. Expert. Rev. Anticancer Ther. 8, 1197-1202. (2008)

4. S. J. Bray, Notch signalling: a simple pathway becomes complex. Nat. Rev. Mol. Cell Biol. 7, 678-689. (2006)

5. A. Zolkiewska, ADAM proteases: ligand processing and modulation of the Notch pathway. Cell Mol. Life Sci., 65, 2056-2068. (2008)

6. B. Varnum-Finney, L. Wu, M. Yu, C. Brashem-Stein, S. Staats, D. Flowers, J.D. Griffin, and I.D. Bernstein, Immobilization of Notch ligand, Delta-1, is required for induction of Notch signaling. J. Cell Sci. 113, 4313-4318. (2000)

7. R. Le Borgne, Regulation of Notch signalling by endocytosis and endosomal sorting. Curr. Opin. Cell Biol. 18, 213-222. (2006)

8. A. Chitnis, Why is Delta endocytosis required for effective activation of Notch, Dev. Dyn. 235, 886-894. (2006)

9. M. Carrion-Vazquez, A.F. Oberhauser, S.B. Fowler, P.E. Marszalek, S.E. Broedel, J. Clarke and J.M. Fernandez, Mechanical and chemical unfolding of a single protein: comparison. Proc. Natl. Acad. Sci. U.S.A. 96, 3694-3699.(1999)

10. W.R. Gordon, D. Vardar-Ulu, G. Histen, C. Sanchez-Irizarry, J.C. Aster, and S.C. Blacklow, Structural basis for autoinhibition of Notch. Nat. Struct. Mol. Biol. 14:295-300. (2007)

11. A.P. Witta, S.R.K. Ainavarapu, H.H. Huang and J.M. Fernandez. Force-dependent chemical kinetics of disulfide bond reduction observed with single-molecule techniques. Proc. Natl. Acad. Sci. U.S.A.103, 7222–7227. (2006)

12. H. Dietz, F. Berkemeier, M. Bertz, M. Rief. Anisotropic deformation response of single protein molecules. PNAS USA, 103, 12724-12728 (2006)

13. K.T. Sapra, P.S.H. Park, K. Palczewski, D.J. Muller. Mechanical properties of bovine rhodopsin and bacteriorhodopsin: Possible roles in folding and function. Langmuir, 24, 1330-1337 (2008)

Appendix A - Noise comparison of traces with and without NORM :

The performance of the AFM (in terms of noise) with and without NORM circuit was studied. These are described in the following two sub sections.

A.1.Comparison of Noise for (A-B)Raw and (A-B)Norm at different values of V(A-B)Raw at FX experimental condition:

Points per trace = 5,000
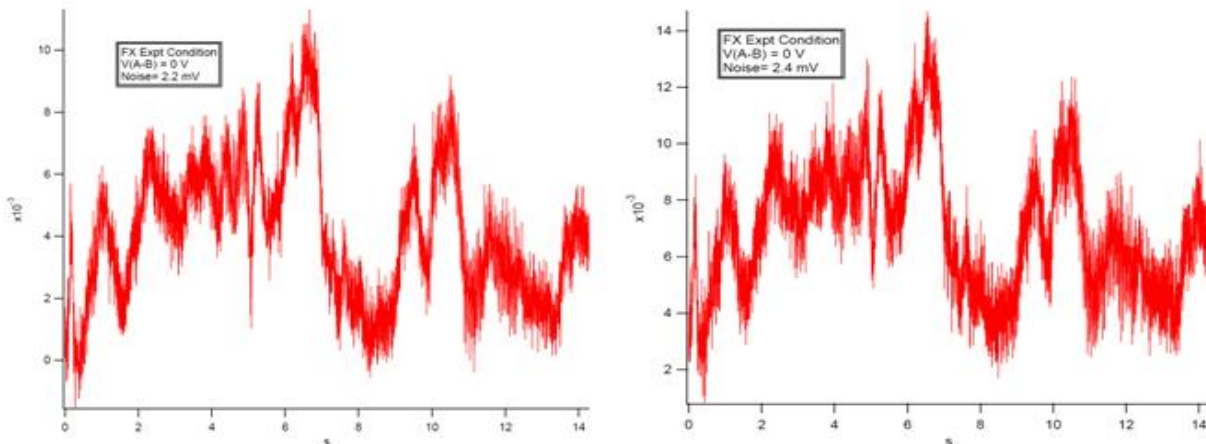Nyquist Fraction = 0.21
Total duration = 3 sec
Effective total duration = Total Duration/Nyquist Fraction = 14.28 sec.
Bandwidth = 350 Hz
V(A+B) = 9.90 V for all cases of study.

V(A-B)	Noise in (mV)	
	V(A-B)	V(A-B)Norm
0	2.2	2.4
1	2.8	3.2
-1	2.4	2.8
2	2.8	4.5
-2	2.2	3.4

Fig. A.1 Sample noise (in mv) vs. time traces in FX experimental condition with and without NORM.

A.2. Comparison of Noise for (A-B)Raw and (A-B)Norm at different values of V(AB)Raw at FC experimental condition:
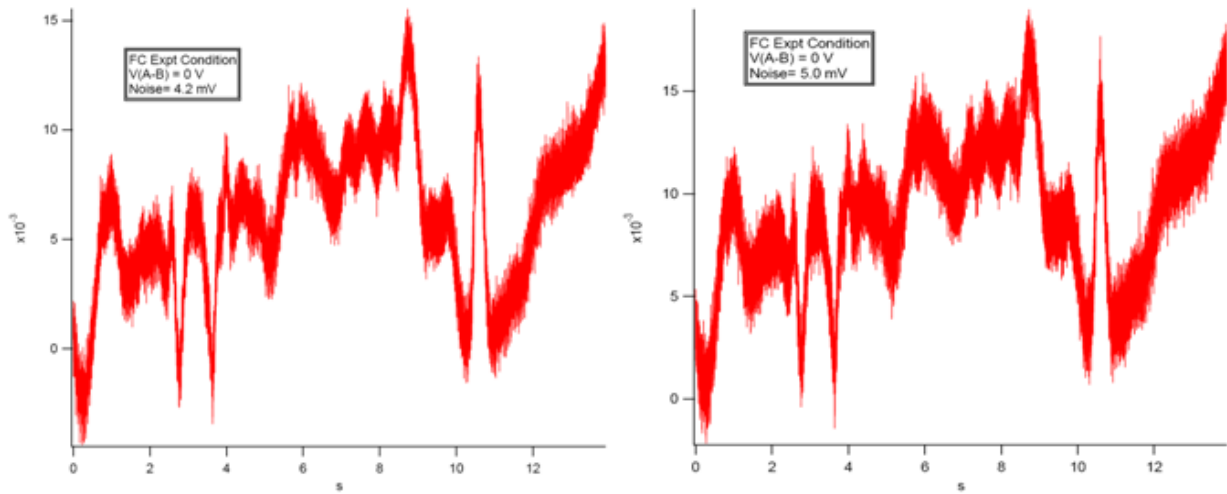
Points per trace = 60,000
Nyquist Fraction = 0.41
Total duration = 5.7 sec
Effective total duration = Total Duration/Nyquist Fraction = 13.9 sec.

Bandwidth = 4316 Hz
V(A+B) = 9.90 V for all cases of study.

| V(A-B)	Noise in (mV)	
	V(A-B)	V(A-B)Norm
0	4.2	5.0
1	4.3	5.2
-1	3.1	3.9
2	3.2	5.0
-2	3.1	5.1

Fig A.2 Sample noise (in mv) vs. time traces in FC experimental condition with and without NORM.

Although, we got more noise with NORM than without NORM, we decided to use the (A-B)Norm signal because of better reliability.

Appendix B: Friction Loop

The surface friction can be found in one direction and in exactly opposite direction on a sample; they can be called forward and backward frictions. These are measured by the forward and backward LFM signals. A figure containing the forward and backward friction forms a loop, is known as a friction loop.
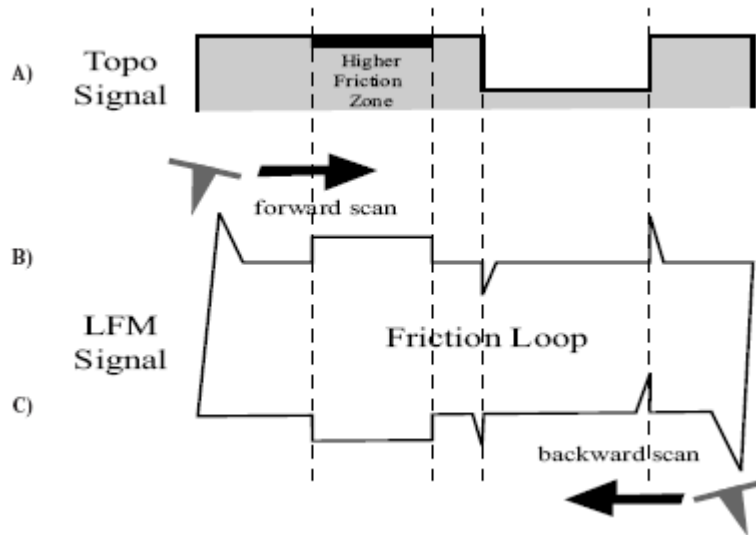
Fig. B.1 (A) The topography signal and (B) the LFM signal in forward direction and (C) LFM signal in backward direction. In (A), dark zone represents the area having higher friction. (B+C) shows the friction loop.

Appendix C: An alternative unfolding scenario for Notch NRR domain

Here, we calculate the values of Lc for the NRR region in an alternative way as presented in section 4.6. We suppose that any units of secondary structure, namely alpha helices and beta sheets, stretch easily at the forces applied in the FX experiments. We also assume that unfolding starts from LNR-A, B, C domains followed by HD domain.

Detachment of LNR-A followed by unfolding up to LNR-B: Distance between the residues 1450-1480 which are "trapped" in between the -S–S- bonds is 1.7 nm. Length of unfolding residues (1481-1490) is 4 nm. Thus, the expected Lc at which detachment of LNR-A occurs is 3.9+1.7+4 = **9.6 nm**

Detachment of LNR-B followed by unfolding up to LNR-C: Distance between the residues 1491-1522 which are "trapped" in between the -S–S- bonds is 1.93 nm. Length of unfolding residues (1523-1528) is 2.4 nm. The expected Lc at which detachment of LNR-B occurs is 9.6+1.93+2.4 = **13.57 nm**

Detachment of LNR-C followed by unfolding up to an –S–S- bond in a HD domain: **A) without unfolding of residues trapped by the S1 site.** Distance between the residues 1529-1562 ("trapped" in between the -S–S- bonds) is 1.93 nm. Length of residues 1563-1622 and 1670-1685, i.e. 76 residues, is 30.4 nm. Expected Lc at which detachment of LNR-C occurs is 13.57+1.93+30.4 = **45.9 nm**. **B) With unfolding of residues trapped by the S1 site.** The length of residues 1563-1685, i.e. 123 residues, is 49.2 nm. Expected Lc is 13.57+1.93+49.2 = **64.7 nm**.

Detachment of HD domain up to the C-terminal: Distance between the residues 1686-1693 which are "trapped" in between the -S–S- bond is 0.74 nm. Length of residue 1694-1727, i.e. 34 residues, is 13.6 nm. Expected Lc at which detachment up to C-terminal occurs is 45.9+0.74+13.6 = **60.24 nm.** Counting the S1 site opening we get 64.7+0.74+13.6 = **79.04 nm.**